

SOLIDIFICATION BEHAVIOUR OF EUTECTIC AND  
NEAR EUTECTIC ALUMINUM-COPPER ALLOYS

by

PRADEEP ROHATGI

S.B., Banaras Hindu University, India, 1961

Submitted in Partial Fulfillment of the  
Requirements for the Degree of

MASTER OF SCIENCE

at the

Massachusetts Institute of Technology

1963

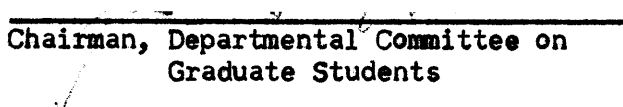
Signature of Author

  
Department of Metallurgy, January, 1963

Certified by

  
Thesis Supervisor

Accepted by

  
Chairman, Departmental Committee on  
Graduate Students

SOLIDIFICATION BEHAVIOUR OF EUTECTIC AND  
NEAR EUTECTIC ALUMINUM-COPPER ALLOYS

by

PRADEEP ROHATGI

Submitted to the Department of Metallurgy on January, 1963,  
in partial fulfillment of the requirements for the  
Degree of Master of Science

---

ABSTRACT

Solidification characteristics of eutectic and near eutectic aluminum copper alloys have been studied over a range of freezing rates. A mathematical theory is developed for freezing of rod shaped dendrites, which is in remarkable agreement with observations on  $\mathcal{L}$  and  $\text{CuAl}_2$  dendrites. Interactions between neighboring dendrites during solidification have also been theoretically analyzed. Side branching characteristics are shown to depend on alloy content and freezing rates, crystallography alone does not govern its morphology.

Lamellar eutectic between  $\alpha$  and  $\text{CuAl}_2$  is found to exist in dendritic form with side branches in addition to colonies observed before. A direct evidence has been presented suggesting that colonies grow with rejection of certain species. A possibility, that mechanism of eutectic solidification actually consists of deposition of one phase in supersaturated form and then precipitation of second from it, is investigated through theoretical analysis and microstructural observations. The model was found to be a possible explanation of the formation of dendritic interface during eutectic solidification and presence of  $\alpha$  envelopes around  $\text{CuAl}_2$  and eutectic dendrites. An electron microprobe investigation shows that the composition of this  $\alpha$  phase is much higher than expected normally from equilibrium considerations.

For the first time a long continuous platelet of  $\text{CuAl}_2$  with lamellar eutectic on its sides has been observed in a eutectic colony formed during slow solidification. A possible explanation for this behaviour is proposed.

Thesis Supervisor: Clyde M. Adams, Jr.

Title: Associate Professor of Metallurgy

## TABLE OF CONTENTS

| <u>Section No.</u> |   | <u>Page No.</u> |
|--------------------|---|-----------------|
|                    | ABSTRACT -----  | i               |
|                    | LIST OF TABLES -----                                    | v               |
|                    | ACKNOWLEDGEMENTS -----                                  | vi              |
| I                  | INTRODUCTION -----                                      | 1               |
| II                 | EUTECTIC SOLIDIFICATION -----                           | 7               |
| III                | THEORY -----  | 9               |
|                    | 1. Dendritic Growth -----                               | 9               |
|                    | A. Mass Transport -----                                 | 9               |
|                    | B. Heat Flow -----                                      | 12              |
|                    | 2. Eutectic Solidification -----                        | 15              |
| IV                 | EXPERIMENTAL PROCEDURES -----                           | 18              |
|                    | A. Preparation of Alloys -----                          | 18              |
|                    | B. Polishing, Etching & Light Microscopy                | 18              |
|                    | C. Preparation of Plates -----                          | 19              |
|                    | D. Arc Deposition -----                                 | 19              |
|                    | E. Quantitative Metallography -----                     | 20              |
|                    | F. Electron Microprobe Analysis -----                   | 21              |
|                    | G. Plaster Castings -----                               | 22              |
|                    | H. Studies of Solidification in Flowing<br>Stream ----- | 23              |



| <u>Section No.</u> |  | <u>Page No.</u> |
|--------------------|--|-----------------|
| V                  | RESULTS AND DISCUSSIONS -----              | 24              |
|                    | A. Hypoeutectic Alloys -----               | 24              |
|                    | B. Aluminum 38 Percent Copper Alloys ----- | 33              |
|                    | C. Eutectic Solidification -----           | 36              |
| VI                 | CONCLUSIONS -----                          | 46              |
| VII                | SUGGESTIONS FOR FURTHER WORK -----         | 49              |
|                    | Appendix I - Interactions Between          |                 |
|                    | Neighboring Dendrites -----                | 49              |
|                    | Appendix II - Mathematical Analysis of the |                 |
|                    | Proposed Model of Eutectic Solidification  | 54              |
| VIII               | TABLES AND ILLUSTRATIONS -----             | 58              |
| IX                 | BIBLIOGRAPHY -----                         | 101             |

## LIST OF TABLES

| <u>Table No.</u> | <u>Title</u>  | <u>Page No.</u> |
|------------------|---|-----------------|
| I                | Composition of Aluminum used for Alloy<br>Preparation -----   | 58              |
| II               | Calculations of Solidification Parameter  | 59              |
| III              | Variation of Dendrite spacing with<br>Solidification Parameter for 24% Copper -                                   | 60              |
| IV               | Variation of Dendrite Spacing with Copper<br>Content at Solidification Parameter Value<br>$\sqrt{q/v} = 10$ ----- | 60              |
| V                | Variation of Growth Constant ( $\beta$ ) with<br>Copper Content -----   | 61              |
| VI               | Variation of Dendrite Spacing with<br>Solidification rate for 28% Copper Alloy                                    | 61              |
| VII              | Variation of Colony Spacing with Solidi-<br>fication Rate in Al-Cu Eutectic Alloys --                             | 62              |
| VIII             | Variation of Interlamellar spacing with<br>Solidification rate in Al-Cu Eutectic ---                              | 63              |
| IX               | Results of Solidification Studies in<br>Flowing Stream -----  | 64              |

### ACKNOWLEDGEMENTS

The author gratefully acknowledges the able guidance and encouragement by Professor C. M. Adams, Jr. during the course of this study.

He also wishes to express his sincere thanks to the staff of M.I.T. Foundry and Welding Laboratories for their help in the experimental phases of the program. He is also very thankful to Miss Frances Gedziun for typing the thesis.

## I. INTRODUCTION

This work includes the studies of solidification behaviour in aluminum copper alloys of eutectic and near eutectic composition. The aim was to examine the characteristics of dendritic growth in melts with high solute content and also to investigate the mechanism of eutectic solidification. These studies are important from the practical standpoint as the distribution of individual phases effects the strength and heat treatment characteristics of a polyphase alloy. The studies on eutectic alloys are useful as these are quite often present in small amounts in dilute engineering alloys; moreover, alloys used as solders are usually of eutectic composition.

Solidification is a two stage process of nucleation and growth. Unfortunately the nucleation behaviour<sup>1,2</sup> in alloy solidification has not been well understood as yet. However, usually under actual freezing conditions because of the presence of heterogeneous nuclei, nucleation is not much of a problem and growth is the important factor governing the

ultimate morphology. Factors effecting the growth characteristics are mainly:

1. Crystallographic considerations.
2. Thermal considerations.
3. Mass transport considerations.

Crystallographic factors are important since now it is well established that solid grows into liquid by successive addition of individual atoms. The ease and rate of addition of one atom to an atomic plane depends upon the atomic distribution on that plane. Thermal considerations come into play because it is necessary to remove the latent heat produced on solidification for continued growth. The overall solidification rate depends on the rate of heat extraction irrespective of the growth mechanism. The problem of mass transport arises because the solid separating from liquid is of a different composition and solute is either manufactured or consumed at the interface depending on the value of distribution coefficient  $K(\frac{C_s}{C_l}$  in Figure 1). Under freezing rates of interest, this solute is not able to diffuse away into the liquid and a concentration profile shown in Figure 2, is obtained.

In Figure 3 the actual temperature distribution and liquidous temperature distribution shows that liquid near to the interface is supercooled. Moreover, the liquid slightly farther away from the interface is more supercooled than that immediately adjacent to it. The solid interface reaches out for this supercooled liquid by developing protrusions so that for the same rate of overall mass growth, the interface area is maximum; hence, the build up of the solute per unit area is a minimum. Rutter and Chalmers<sup>3</sup> have discussed how the form of protrusions is effected by the ratio of temperature gradient (G) to the rate of growth (R). They show that at small rates of G/R these take the form of dendrites.

Thus we see that the localized growth rate is governed by the mass transport problem whereas the overall solidification rate depends upon rate of heat removal.

Most of the work done on dendritic growth is qualitative. Three aspects of dendritic growth, namely the crystallography, the spacing between dendrites (the lateral growth), and the longitudinal growth rate seem to be the most important characteristics. It has been well established that

dendrites<sup>4,5</sup> grow in the direction resulting from the growth on most densely packed planes. During dendritic growth there is no simple relation between overall rate of movement of solid liquid interface and mass freezing rate. However, quantitative solutions to linear growth rates of individual dendrites have been presented by several workers<sup>7</sup>. We shall discuss mainly the problem of spacing between the dendrites.

Brown<sup>7</sup> has presented a quantitative relationship for the dendrite spacing which is in good accordance with the experimental results on several alloys. This analysis predicts an increase in dendrite spacing with diffusivity, freezing time and degree of supercooling.

The predictions appear physically reasonable that with increase in diffusivity, or decrease in freezing rate the rate of solute accumulation is less; hence, for the same growth rate lesser numbers of dendrites (implies a lesser surface area) would be able to accommodate the solute. Similar relationship between diffusivity freezing rate and dendrite spacing is observed by French<sup>8</sup> in the case of solidification of ice. The prediction of Brown<sup>7</sup> regarding

the effect of supercooling appears to be quite sound, that more the amount of supercooling liquid can sustain, more solute it will accommodate and, hence, the farther spaced the dendrites can be. However, their observation that the supercooling is independent of cooling rate is probably because of the experimental conditions used in which nucleating surface was already present.

The story of dendritic crystallization is not complete without understanding the later stages in lateral growth after the establishment of primary dendrite spacing. The interdendritic liquid goes on getting richer in the solute content due to separation of primary phase until finally it reaches the eutectic composition after which probably it solidifies as such. The exact mechanism of nucleation and growth of this eutectic is not quite clear; also, in some cases one of the eutectic phases is nucleated and deposited on the primary dendrites and we observe only the second phase in the interdendritic region. However, if during growth, conditions in liquid change in a manner necessitating a smaller dendritic spacing, secondary arms develop on these primary dendrites. The quantitative information regarding these secondary arms is not very satisfactory.



In the present work a more sophisticated relationship for dendrite spacing, considering rod shaped dendrites, has been developed. Also, attempts have been made to study the effect of solidification of a dendrite on its neighbor. High copper, aluminum copper alloys are used to see whether the relationship holds good in near eutectic compositions and also to observe the effect of increased concentration on the dendrite morphology.

## II. EUTECTIC SOLIDIFICATION

The mechanism of eutectic solidification has not been well understood in spite of the large number of years which have elapsed since it was first observed. However, several classifications<sup>9,10,11</sup> of eutectics have been developed which are based either on the shape of the phase particles or on the degree of association between the two phases. The basic concepts are still more or less same that the two phases either nucleate side by side and then grow into the melt or they nucleate separately, independent of each other and then come into contact and grow simultaneously. Vadilo<sup>12</sup> calls it as the interlaced dendritic growth of two crystals of different phases. Tiller<sup>14</sup> has treated the problem quantitatively and has predicted the possible interface shape and the variation of interlamellar spacing with freezing rates.

Weart and Mack<sup>15</sup> have discussed the difference between eutectic colonies, grains and lamella. They have found colonies to be a common growth feature in several eutectics. Interestingly enough, their observations show that orientation of one phase ( $\mathcal{L}$  in  $\mathcal{L}$ -CuAl<sub>2</sub> eutectic) was same over several colonies, an

observation comparable to same orientation of several dendrites in a grain. They have proposed that colony structure is generated because the plane front breaks down into cellular interface due to some common impurity rejected by both phases; these cells grow into colonies. On this postulation, they have explained the fanning and coarsening of lamella at the colony boundaries. Craft and Albright<sup>16</sup> have also verified this theory of colony formation and also have observed several defects in lamellar structure. Above theories seem to be quite adequate at the surface but do not explain several facts like the continuity of a certain phase in a eutectic, also the break down of lamellar structure at the colony boundary and in the regions between colonies.

The present work involves a quantitative study of colony structure in Al-CuAl<sub>2</sub> eutectic alloys. Several unique structures were observed during the studies especially with slow solidification rates and a theory is proposed for colony formation which helps to explain the results. The essence of the theory is that only one of the two phases deposits from the liquid during the growth process and the second phase is formed by a solid state precipitation process rather than a simultaneous growth in liquid.

### III. THEORY

#### 1. Dendritic Growth

##### A. Mass Transport.

We have discussed earlier that dendrite formation can be visualized as sudden development of protrusions in liquid and their lateral growth in the melt. Thus we can approximate a dendrite in its initial growth stages as a line source rejecting solute atoms in an infinite medium. The equation derived by Carslaw and Jaeger<sup>17</sup> for heat flow in an infinite medium from a continuous line source is:

$$T - T_0 = \frac{q}{4\pi\mathcal{L}\rho c_{p1}} \int_{\frac{r^2}{4\theta}}^{\infty} \frac{e^{-u}}{u} du$$

(Equation 1)

where:  $T_0$  = Initial temperature of the mass.

$T$  = Temperature at radius  $r$ .

$q$  = Heat quantity liberated per unit time.

$\rho$  = Density.

$c_{p1}$  = Specific heat of liquid.

$\theta$  = Time.

$\mathcal{L}$  = Diffusivity.

By similarity, we can write the equation for mass flow around a continuous source rejecting solute (Figure 4).

$$C - C_0 = \frac{n}{4\pi D_1} \frac{r^2}{4D_1\theta} \int_0^{\infty} \frac{e^{-u}}{u} du$$

(Equation 2)

Where:  $C_0$  = Initial concentration of liquid.

$C$  = Concentration at radius  $r$ .

$D_1$  = Diffusivity in liquid.

$\theta$  = Time.

$n$  = Number of solute atoms rejected per unit time.

Using  $r_s$  for the radius at time  $\theta$  of the solid region and assuming a parabolic growth rate, we define a constant  $\beta$ .

$$\beta^2 = \frac{r_s^2}{4D_1\theta}$$

(Equation 3)

We now solve equation number 2 with two boundary conditions:

1. At  $r = r_s$   $C = C_L$  {In the very initial stages of freezing.}
2. Mass Balance - Under steady state conditions the

amount of solute rejected at the solid liquid interface is diffused away into the surrounding liquid or

$$c_L (1-K) \frac{dr_s}{d\theta} = - D_1 \left( \frac{\partial C}{\partial r} \right)_{r = r_s}$$

(Equation 4)

Evaluating  $\frac{dr_s}{d\theta}$  from equation 3 and  $\left( \frac{dC}{dr} \right)_{r = r_s}$  from equation number 2 and substituting in equation 4 we get

$$c_L (1-K) \beta = \frac{n}{4\pi D_1} \frac{e^{-\beta^2}}{\beta}$$

(Equation 5)

Evaluating the value of n by applying equation 2 at

$r = r_s$

$$c_L - c_0 = \frac{n}{4\pi D_1} \frac{e^{-\beta^2}}{\beta} d\beta$$

(Equation 6)

From equations 5 and 6

$$\frac{c_L - c_0}{(1-K)c_L} = \text{Ei}(\beta^2) \beta^2 e^{\beta^2}$$

(Equation 7)

where:

$$Ei(\beta^2) = \beta \frac{e^{-\beta^2}}{\beta^2}$$

We can see from equation 7 that the growth constant  $\beta$  depends on the value of initial concentration  $C_0$  and the extent of undercooling which governs  $C_L - C_0$ . Solving equation 7 by trial and error for different values of undercooling we get a relationship between  $\beta$  and  $\Delta T$  represented by Figure 5 for  $C_0 = 4.5$ . This curve shows that  $\beta$  increases with supercooling almost linearly except for very small values of  $\Delta T$ .

#### B. Heat Flow.

The following relationship is obtained by performing a heat balance between overall rate of heat extraction and the latent heat liberated by dendrites freezing with a growth constant  $\beta$ . The dendrites are assumed to be arranged at the centers of a hexagonal network which is a reasonable approximation for rod shaped dendrites.

$$\rho_c p \frac{dT}{d\theta} = \frac{8\sqrt{3}\beta^2 D \rho H}{\sqrt{3} X^2}$$

(Equation 8)

where: X = Dendrite spacing in feet.

D = Diffusivity in ft.<sup>2</sup>/ second.

H = Latent heat of freezing B.Th.U./lb.

C<sub>p</sub> = Specific heat  $\frac{\text{B.Th.U.}}{\text{lb.} \times \text{sec.}}$

$\rho$  = Density of solid or liquid in lbs./ft.<sup>3</sup>

(We neglect density difference between solid and liquid.)

From the above relationship we see that dendritic spacing X is inversely proportional to the square root of the rate of heat extraction and directly proportional to the diffusivity and latent heat of freezing.

In our work the alloys were solidified under a traveling arc (see details later in the chapter of experimental procedures) and the rate of heat extraction for that set up is given by<sup>18</sup>

$$\frac{dT}{d\theta} = 2\lambda K \left(\frac{v}{q}\right) (T_m - T_o)^2$$

(Equation 9)

where: K = Thermal conductivity.

v = Arc travel speed.

T<sub>m</sub> = Melting point, solidous temperature of the metal.

T<sub>o</sub> = Initial temperature of the metal before deposition.

q = Arc power input.



From equations 8 and 9

$$x = \sqrt{\frac{4\beta^2 DH}{1.73 C_p K (T_m - T_o)^2}} \cdot \sqrt{\frac{q}{v}}$$

(Equation 10)

Thus for constant value of  $D$ ,  $H$ ,  $C_p$ ,  $K$  and  $(T_m - T_o)$ , the dendrite spacing should be a linear function of  $\sqrt{\frac{q}{v}}$ . The work of Brown<sup>7</sup> on several alloys is in accordance with this theory. A calculation was made by substituting the data of obtained by him on 2014 alloys in equation 10 (the values of other constants were taken from reference 7) giving the value of  $\beta$  to be equal to 0.05 (which is a quite small number) indicating that growth rate of individual dendrite is quite small as compared to overall growth rate.

It appears necessary to investigate the mutual interaction between neighboring dendrites during the solidification process to check the validity of our assumption. A mathematical treatment is presented in Appendix I dealing with two neighboring dendrites freezing simultaneously. It is shown that quite soon during the solidification process (when fraction of solid is 0.0016) the dendrites become aware of each other and each one

should be considered as freezing in a definite zone of liquid around it, rather in a infinite medium. However, it is evident that this condition develops only after the primary dendrite spacing is established; hence, the theory presented for the same remains unaffected. The other implication of this result is that it indicates that the conditions in the liquid change drastically immediately after the protrusion of primary dendrites and the secondary dendrites can form during very early stages of solidification. This is probably the reason that the difference in thicknesses of primary and secondary dendrites is not very large.

## 2. Eutectic Solidification.

The theory proposed here for eutectic solidification postulates that during eutectic solidification only one phase deposits as a supersaturated solid solution and the second phase precipitates from this during growth process resulting in the eutectic structure.

In case of  $\mathcal{L}$  (Al)-CuAl<sub>2</sub> eutectic, quite often the  $\mathcal{L}$  phase is continuous so it is concluded that probably this is the phase which nucleates from the eutectic liquid. However,

even if both phases are present, there will be a tendency for this phase to overlap the  $\text{CuAl}_2$  phase during the growth process. In Figure 8, we consider two phases growing simultaneously into the liquid. The numbers refer to the copper percentages which are taken from extended phase boundaries of equilibrium diagram (Figure 7). (To elucidate the principles, very large supercooling is assumed and the numbers are hypothetical.) It can be seen that copper will try to diffuse out in both liquid and solid from the interface BC. This will cause it to move faster in comparison to BD where copper comes from liquid only. Figure 9 illustrates how this differential growth rate leads to the enveloping of  $\text{CuAl}_2$  phase by  $\mathcal{L}$ .

In Appendix II a mathematical analysis of the proposed model of eutectic solidification (involving the precipitation of second phase from the supersaturated solid solution of the first) is presented. The results indicate that the growth rate of eutectic front by this mechanism is very slow, and therefore, a large number of such fronts will be needed to get an appreciable rate (overall) of solidification corresponding to the rate of heat extraction. This could be a possible explanation for the observed decrease in the size of eutectic colonies with increase in freezing rate.

However, it might be once again stressed that the above theory does not propose any mechanism for the nucleation of eutectic alloys. Also, it can be applicable only in the early stages of solidification; otherwise, the concentration of liquid by continuous rejection of  $\mathcal{L}$  phase would reach very high values. The above theory would require an envelope of  $\mathcal{L}$  phase around every eutectic colony, and the envelope should increase with decrease in solidification rates.

#### IV. EXPERIMENTAL PROCEDURES

##### A. Preparation of Alloys.

The alloys investigated were aluminum-copper alloys with 24, 33 and 38 percent copper respectively. These alloys were prepared by first making a 50-50 hardener in an induction furnace using electrolytic copper and aluminum of composition given in Table I. The hardener was remelted in an induction furnace and diluted with aluminum to get the required composition. Care was taken at every stage to avoid gravity segregation.

##### B. Polishing, Etching and Light Microscopy.

Initial polishing was done on standard rough polishing papers and the final polishing on coarse and fine diamond wheels or the syntron polisher. The alloys being brittle were not hard to polish like the dilute aluminum alloys. The specimens were etched with 25 percent Nitric acid which etched  $\text{CuAl}_2$  phase dark, thereby, giving a better contrast as compared to the regular Kellars reagent. Metallography was done on Riecherts Metallograph, oil immersion lenses used for high magnifications.

### C. Preparation of Plates.

The plates for arc deposition were made by melting the alloy of required composition and pouring it into a mold 1 ft. x 1 ft. x 2 in. which was made by assembling steel plates 1 inch thick. This arrangement produced chilled plates with columnar crystals growing from the bottom and the sides. Horizontal and vertical sections were taken from the plate to examine the nature of dendritic growth in the plates.

### D. Arc Deposition.

Arc deposits were made on the plates described above to investigate solidification behaviour under fast cooling rates. An electric arc is produced between the plate surface and a permanent Tungsten electrode in an atmosphere of Argon to avoid any oxidation. The Tungsten electrode is then moved over the plate surface in a straight line. The apparatus has been described by Ross<sup>22</sup>; a schematic is given in Figure 11. In this case the metal is melted under the arc and then allowed to freeze rapidly by heat extraction through the remaining plate. The arc length is maintained constant automatically.

The time to solidify for the metal melted is proportional to the energy input per unit length of the deposit. This is dependent on the arc power and travel speed. A suitable combination of voltage and current was found resulting in a stable arc. The travel speed was varied between 5 to 95 inches per minute, thereby, varying the cooling rate by almost 18 times. Table II illustrates the calculation of  $\sqrt{q/v}$  values for the conditions used in present work. A microscopic examination was carried out on specimens taken out of these plates. Sections of the material parallel to the weld direction and perpendicular to the plate are referred as vertical sections and those which are parallel to weld direction and parallel to plate are called horizontal sections (Figure 12).

#### E. Quantitative Metallography.

Dendrite spacings and interlamellar spacing were measured on these arc deposits. All the measurements were made in the immediate vicinity of weld interface because the cooling velocity increased with distance from this interface. Spacing measurements were made on dendrites perpendicular to the interface by counting the number of dendrites along certain length of the interface. Several sets of observations were taken and a statistical average was found out.

#### F. Electron Microprobe Analysis.

Electron microprobe analysis was performed on the specimens from chilled cast plates with 38 percent copper. The aim was to determine the composition of the envelope of  $\delta$  phase which was invariably found to be present around  $\text{CuAl}_2$  particles in these alloys. Unetched specimen polished on a syntrom was placed in the probe and irradiated by the electron beam. The scanning crystal was so adjusted that out of the emitted copper and aluminum radiations only copper radiations were reflected and fed into the counter. The geared motor was switched on which moved the specimen along a straight line at a fixed speed. This enables us to determine composition along a certain length of the specimen. The sample when examined later showed a light streak along the path traversed by the beam. A light etch clearly revealed its entire path as well as the structure it had analyzed. Copper percentages were calculated from the intensity recording chart assuming the intensity - composition scale to be linear specially at low copper percentages. The observations on aluminum-copper system done elsewhere<sup>23,24</sup> also support this assumption.



### G. Plaster Castings.

In order to obtain slow solidification rates, plaster molds were used for freezing the alloys. Circular molds, 5 inches in diameter, 5 inches in height with a cylindrical cavity 1.6 inches diameter, and 2.8 inches in length in the top portion, were made from casting plaster by standard techniques. These molds were preheated in a gas fired furnace for 48 hours at 500°F. Alloy chips were kept into the cylindrical cavity of the mold and melted by a welding torch. The melt was superheated sufficiently and stirred by a tungsten rod to avoid any segregation. The molten pool was then allowed to solidify. With such an arrangement, a unidirectional solidification is obtained by extraction of heat into air as on the rest of the sides the melt is surrounded by insulating plaster. Ingots frozen in this manner showed dendrites growing from top surface downwards. In some cases, additional heat was supplied from top by weld torch to obtain still slower solidification rates. The cast rod was taken out and sectioned through the center along the length and polished for metallographic examination.

#### H. Studies of Solidification in Flowing Stream.

An apparatus was developed to study the solidification behaviour of alloys in a flowing stream. The equipment<sup>25</sup> shown in Figure 13 mainly consists of an inclined trough of steel with a water jacket at the bottom for chilling. Alloy melts from induction furnace after being sampled were poured down the trough. The solidified strip was removed and the overflowed metal was collected in another crucible at the bottom, sampled and repoured again over the trough. The process continued until no more metal overflowed. Samples for chemical analysis were taken from the solid strip at one foot intervals from pouring end. Also the samples collected from initial liquid and the remains after each pour were chemically analyzed. Metallographic examination was conducted on solid strips taking specimens along a plane perpendicular to the strip along the length of the pour.

## V. RESULTS AND DISCUSSIONS

### A. Hypoeutectic Alloys (24% Copper).

The 24 percent alloy chilled cast plates solidified directionally from the bottom as shown by Figure 14 which is a vertical section of the plate showing dendrites of  $\alpha$  phase with eutectic in between. Some of the dendrites appear to be well developed having secondary as well as tertiary branches (Figure 15). The secondary arms appear to almost perpendicular primary arms, whereas the tertiary ones are inclined at an angle slightly less than  $90^\circ$ . A horizontal section across the dendrites (Figure 16) indicates that these have a four fold symmetry. Similar dendrites of the  $\alpha$  phase have been found in chill cast 4 percent copper alloys<sup>26</sup>, but without so extensive tertiary branching.

The arc deposits of this alloy show a transition zone (Figure 17) at the interface between original plate and rapidly frozen weld deposit. The transition zone contains coarse primary  $\alpha$  particles, of the same size as in the original plates, with a very fine eutectic in between. This happened because in this region only partial melting of plate occurred; only the eutectic melted and the primary particles remained as such.

The liquidated eutectic froze with fine lamellar structure. Next to the transition zone is rapidly frozen zone exhibiting fine dendrites of  $\alpha$  phase. The dendrites have nucleated perpendicular to the interface so the vertical sections of the specimens show longitudinal sections across them (Figure 18). The dendrite spacing and the interlamellar spacing of the interdendritic eutectic both decreased as we moved into the welded zone away from the interface. This indicates that in the weldments the cooling velocity is slowest at the interface compared to normal sand castings where it is maximum at the mold interface.

A horizontal section of the arc deposit showed very long dendrites of  $\alpha$  phase in the center extended along the weld direction (Figure 19). These long dendrites were slightly discontinuous along the ripples but had a tendency to grow in the same direction even after the interruption. It might be mentioned here that weldments showed curved ripples which are the planes along which the solute deposited periodically due to supersaturation at the solidification front. These long dendrites found in the horizontal section near the top of the welds are formed probably because during the period the

dendrites were growing from all sides of the semicircular interface, the liquid in the center of the circle near the top cooled and started freezing before the dendritic solidification front could reach it. This gave rise to dendrites which grew parallel to the weld direction independent of the interface.

The shape of the dendrites in the arc deposits is different from the cast plates. Here it consists of one long stem with rods attached to the sides of it making an angle of almost  $60^\circ$  to the main axis. Twelve of these side branches appear to project from a point on the main stem arranged at an angle of  $30^\circ$  to each other as indicated by a transverse section across a dendrite (Figure 20). Also the side branches were much smaller in relation to the main stem in this case as compared to chilled cast plates. Hence, it is concluded that with increase in solidification rate the primary dendrites are placed closer; there is an increase in the number of secondary arms projecting from a point but at the same time a decrease in relative length of secondary arms. The growth direction of the secondary arms appears to change to one of larger fold symmetry with increase in solidification rates.

Interesting observations regarding the effect of solute concentration on dendrite shape are made when dendrites obtained in the present work are compared to the dendrites obtained by Brown<sup>7</sup> on 4.5 percent copper alloys. Brown<sup>7</sup> did not observe any side branching in 4.5 percent copper arc deposits under similar freezing rates, where as the presence of the side branching in some alloys under slow freezing conditions has been mentioned before<sup>26</sup>. This observation indicates that tendency of side branching increases with the solute content. The absence of side branching in 4.5 percent copper alloy arc deposits may be due to the fact that rapid freezing rates reduced the length of side branches to nothing because of lesser tendency of side branching at low alloy contents.

The quantitative metallography results on arc deposits of these alloys show a linear variation of dendrite spacing with the solidification parameter  $\sqrt{q/v}$  (Figure 22) Table III. This is in accordance with the proposed theory that dendrite spacing increases linearly with the square root of freezing time. Figures 21, 23 and 24 illustrate the decisive role of freezing rate on dendrite spacing.

The values of dendrite spacings at a fixed solidification rate ( $\sqrt{q/v} = 10$ ) for several aluminum-copper alloys are presented in Table IV. A plot of dendrite spacing versus copper percentage shows a linear relationship between the two (Figure 25). This result is in accordance with the observations of Alexander who found increase<sup>27</sup> in dendrite spacing, for several alloys, with solute content. French<sup>8</sup> also observed a similar relationship for ice dendrites during solidification of water. A plot from his data is presented in Figure 26 showing linear increase in dendrite spacing with KCl content.

The dendrite spacing of  $\text{CuAl}_2$  in 38 percent alloys is only 13 microns at solidification parameter value of ten (same as that of hypoeutectic alloys, Figure 25). This indicates that the dendrite spacing increases with solute content only till the eutectic composition. This is also expected because after eutectic composition the primary phase appearing as dendrites is different and in this case may have a low characteristic spacing (the spacing to which the plot between solute content and dendrite spacing extrapolates at zero solute contents is referred to as characteristic spacing<sup>25</sup> it is probably the same irrespective of solute considered). However, the dendrite

spacing for 38 percent alloy fits the straight line for hypoeutectic alloys if, instead of copper content,  $Co-C_s$  (the amount of solute to be rejected at the outset of freezing) is plotted against dendrite spacing. As this change would not effect the plot for hypoeutectic alloys appreciably (also will have no effect on ice data since  $C_s = 0$ ), the spacing for 38 percent alloys is plotted on the original graph (Figure 25).

This indicates that dendrite spacing might be a function of  $Co-C_s$  for the same system independent of the primary phase separating out. Equal dendrite spacing observed by Brown<sup>7</sup> in copper-nickel alloys with 30 percent and 60 percent nickel, respectively, indicates that dendritic spacing does not depend on impurity content only. Also the fact that these alloys have almost the same  $Co-C_s$  value suggests that dendrite spacing may be function of composition difference between liquid and first separating solid in a system. However, it should be mentioned that these observations might be just a fortunate coincidence due to interplay of several other factors and more systematic investigations should be made confirming this dependence.



The increase in dendrite spacing with the amount of solute to be rejected as observed in present work does not comply with our theory. This is because the larger the amount of solute to be rejected, more must be the number of dendrites for the same overall solidification rate, so that the growth rate and, hence, the increase in solute accumulation per unit area of individual dendrites is the same. This leads to the conclusion that change in some other parameter also exercises its influence to offset this effect.

From equation 10 we know:

$$\frac{X}{\sqrt{q/v}} = \frac{K' \beta}{T_m - T_0} \sqrt{\frac{DH}{C_p K}}$$

If we assume that the factor  $\sqrt{\frac{DH}{C_p K}}$  does not change appreciably with copper content then we can rewrite the above equation as:

$$X = \frac{K'' \beta}{T_m - T_0}$$

(Equation 32)

for a constant value of  $\sqrt{q/v}$ .

Equation 32 indicates that a change in dendrite spacing with concentration of solute is due to a change in

the value of  $\beta$  (the change in  $T_m - T_o$  with solute concentration is hardly of the order of 15-20 percent). A calculation taking the value of constant  $K''$  same for all alloys (same as that for 4.5 alloy<sup>7</sup>) resulted in the values of  $\beta$  (Table IV) showing almost a five fold increase with change in copper concentration from 1 to 24 percent.

We know from equation 7:

$$F(\beta) = \frac{C_L - C_o}{C_L - C_s} = \frac{\Delta T}{(C_L - C_s)m}$$

(Equation 33)

where  $F(\beta)$  is an increasing function of  $\beta$ ,  $\Delta T$  the supercooling and  $m$  the slope of the liquidus. From equation 33, it is obvious that an increase in  $\beta$  with  $C_o - C_s$  ( $C_o - C_s \cong C_L - C_s$ ), as observed, is possible only if the supercooling increases with this parameter. A rough estimate indicates that a three fold increase in the value of  $\beta$  with a five fold increase in  $C_o - C_s$  (considering 4 and 24 percent alloys) can result only by about a twelve fold variation in the value of  $\Delta T$ .

There is lack of direct experimental data on the supercoolings in metallic alloy systems<sup>28</sup>. However, direct observations have been made by Grenchy<sup>13</sup> on nonmetallic solutions and melts, showing an increase of supercooling with solute content. It would be interesting to do some direct measurements on supercooling of alloy melts without allowing any heterogeneous nucleation (in this case the effect is observed in spite of the presence of pre-existing nucleating surface). The observed effects of increase in supercooling with difference in solid liquid composition may be due to increased diffusion requirements which probably offset the effect of increased free energy difference.

The solidification of the interdendritic liquid will be discussed during considerations of eutectic solidification because here we have eutectic in between primary dendrites rather than  $\text{CuAl}_2$  as was observed in arc deposits<sup>7</sup> of 4.5 percent copper alloy. Also there appears to be a boundary of  $\text{CuAl}_2$  between primary  $\alpha$  and the eutectic.

### B. Hypereutectic Alloys.

The 38 percent copper chilled plate freezes with a dendritic structure as shown by Figure 27. The fine structure in the picture is of the arc deposited material in the plate. The dendrites appear to be very uniformly arranged and appear to have a three fold symmetry. Figure 28, which shows transverse section of a cross the dendrites clearly reveals the striking three fold symmetry in which the secondary branches are arranged about the main stem which appears to be a rod.

Investigation of the arc deposits in these alloys show a transition zone like 28 percent alloys (Figure 29), however, in this case the  $\text{CuAl}_2$  dendrites, in the arc deposits have the same shape as in plates. A vertical section through the arc deposits (Figure 30) throws further light on the shape of the  $\text{CuAl}_2$  dendrites. It appears that these consist of a long rod with three secondary branches projecting from points along its length. The three side branches are inclined to the main stem at an angle of  $60^\circ$  and are symmetrically arranged around it, making angles of  $120^\circ$  with each other. Very small tertiary branches are also observed.

The crystal structure of  $\text{CuAl}_2$  is complex body centered tetragonal, a prototype of C16 type<sup>29</sup>. Growth on any of the close packed planes, symmetrical about the tetragonal axis could have lead to the formation of the main stem. However, the three fold symmetry of secondary branches is unexpected because in a tetragonal crystal there is no such symmetry. A possible explanation could be that this structure represents growth along directions with four fold symmetry as all the branches are inclined to each other at  $120^\circ$ . Excessive growth along one of the four axis due to heat extraction in that direction could have resulted in the observed structure. Direct X-ray investigations are necessary to establish the crystallography of growth in this system.

At this point, it seems worthwhile to mention an interesting visual observation. The chilled cast plate of 38 percent alloy showed a peculiar tearing at the top surface which froze last (Figure 31). The surfaces of 4, 24 and 33 percent copper plates cast under similar conditions were more or less smooth. This indicates that this occurrence is not due to shrinkage of the interdendritic liquid but is an outcome of properties of the primary phase. The commonly observed three

fold symmetry of the tears indicates a possible correlation to the dendrite shape, although such a direct dependence appears unlikely. The tearing is probably caused by the shrinkage of dendritic network of  $\text{CuAl}_2$  during cooling.

Coming back to the arc deposits in 38 percent alloy, the relation between dendrite spacing and the square root of freezing velocity is linear in this case too (Table VI, Figure 32). Thus the proposed theory holds equally well whether the solidification front is rejecting or consuming solute. Figures 33 and 34 show the effect of cooling rate on dendrite spacing and the remarkable uniformity in the pattern of arrangement. Figures 35 and 36 represent two unusual structures observed during the metallography. Figure 35 shows abnormally large secondary branches with well developed tertiaries and Figure 36 shows unusually long dendrites running across the picture.

Another interesting feature of  $\text{CuAl}_2$  dendrites in 38 percent alloys is that they are usually surrounded by an envelope of  $\alpha$  phase (Figures 29 and 37). The thickness of the envelope appears to decrease with increase in solidification rate. An electron-probe beam was run across the  $\text{CuAl}_2$

dendrites in order to investigate the copper content of the  $\alpha$  envelopes (Figures 38 and 39). The white streak represents the path of the beam. Surprisingly enough, the composition of the  $\alpha$  phase in these structures was 8-9 percent copper instead of 4.5 percent. It appears that the presence of these envelopes is not an outcome of dendritic crystallization but probably is associated with the mechanism of the solidification of the interdendritic liquid.

### C. Eutectic Solidification.

The chilled cast plates of 33 percent alloys froze with eutectic colonies growing upwards from the base of the chill. Figure 40, a vertical section of the plate, shows the eutectic grown exactly in a manner similar to dendritic crystallization (the white portion in the picture is the unresolvable structure in the arc deposited zone). Side branching from main stem can also be seen. Examination at a higher magnification (Figure 42) reveals that these are colonies arranged in a fir tree pattern, characteristic of dendrites. A horizontal section of the plate show the plan of these dendrite-like colonies (Figure 43). The structure of eutectic in between these colonies is quite coarse and irregular.

A very slow cooled plaster case of 33 percent alloy also showed dendrite-like arrangement of eutectic colonies but with lesser side branching (Figure 41). In this case colonies are still farther apart and the amount of coarse eutectic with irregular particle distribution is considerable.

The arc deposits on the 33 percent plates show eutectic colonies grown perpendicular to the interface (Figure 44). The transition zone is not present in this case because there was no partial melting. However, colony formation is not quite obvious in the immediate vicinity of the interface (Figure 45) which shows lamella grown perpendicular to the interface without any colony formation. Only a little farther away these lamella appear to arrange themselves in colonies.

A quantitative study of variation in the colony spacing with square root of freezing rate showed a linear relationship like the dendrites (Table VII, Figure 46). A comparison of Figure 44 and Figure 47 shows the effect of solidification rate of colony spacing and lamellar spacing as well. A plot between interlamellar spacing and the square root of freezing rate is shown in Figure 48A(Table VIII). Interlamellar spacing increases



with square root of freezing rate but the variation is not exactly linear as predicted by Tiller<sup>11</sup>, especially at slower freezing rates.

The boundaries of the colonies are arranged in a direction parallel to the direction of heat extraction, but the lamella apparently does not seem to be aligned in any particular direction (Figures 45 and 48). Moreover, lamella within a colony appears to differ in spacing and growth direction. Figures 50 and 51 elaborate these facts; in addition, show that in certain colonies the lamella have a tendency to bend about a certain axis. This tendency may be a primary stage in formation of continuous  $\text{CuAl}_2$  platelet along the length of the colony (Figure 54) observed in slow cooled eutectics.

The lamellar arrangement in two colonies in Figure 50 seems to support the overlapping mechanism of eutectic growth proposed by Tiller<sup>14</sup>. Figure 50 also shows some of the defects in lamellar structure discussed by Craft and Albright<sup>16</sup>. One can clearly note the splitting up of one lamella into two at some places; at others, the lamella are discontinuous. It

might be mentioned that Figure 44 shows transverse banding effect even at very rapid freezing rates, hence, it is a defect associated not only with slow freezing rates<sup>16</sup> as suggested before.

One can easily note in these pictures that colonies appear to be separated by an envelope of  $\alpha$  phase from each other. The  $\text{CuAl}_2$  lamella become coarse at the colony boundaries and are separated by a layer of  $\alpha$  phase from the lamella of another colony. All the above unusual observations cannot be attributed as sectioning effects, as proposed elsewhere<sup>13</sup>, and need an investigation in the light of present concepts of eutectic crystallization.

The occurrence of colonies perpendicular to interface in the arc deposits seems to comply with the theory of colony formation proposed by Weart and Mack<sup>15</sup>. The tendency of lamella to arrange themselves into colonies at a small distance away from the interface is because initially they grow with a plane front but quite soon the impurities accumulated and cause formation of cellular interface giving rise to colonies. The fact, that colony spacing obeys remarkably well the theory proposed the dendrite spacing, is also an indirect support because

basically the cell formation and dendrite formation are similar phenomenon, only different in degree.

However, the existence of lamellar eutectic (Figures 40 and 41) in classical dendritic form with side branches cannot be explained simply on a basis of formation of cellular interface. Instead it appears that solidification front breaks down in the form of dendrites which later on developed side branches. The theory of cell formation is inadequate to explain the occurrence of large amount of irregular eutectic in between these dendrite-like particles (Figure 43). Therefore, it appears that eutectic grows in dendritic form like primary phase of any other alloy complying to the heat extraction requirements and the interdendritic liquid, which is also of the eutectic composition, freezes later giving rise to an irregular coarse eutectic.

Coming to the cause of dendritic breakdown of the solidification front, it could be any foreign impurity rejected by both eutectic phases. A similar proposal is made for colony formation<sup>15</sup>, also the absence of colonies in eutectic made from zone refined material<sup>30</sup> offers a strong support to the

viewpoint. However the presence of  $\alpha$  envelopes around  $\text{CuAl}_2$  dendrites of 38 percent copper alloy; the presence of  $\alpha$  envelopes around the eutectic colonies gave rise to the suspicion that probably it is the  $\alpha$  phase which deposits from the liquid during solidification, and the  $\theta$  phase precipitates from this supersaturated  $\alpha$  in such a manner so as to give rise to a eutectic type structure. It was thought that the rejection of copper due to the formation of this supersaturated lead to the breakdown of solidification front giving rise to dendrite shaped particles of eutectic.

The electron probe results, that the  $\alpha$  envelopes around  $\theta$  particles in 38 percent copper alloy plates (Figures 38 and 39) contain 9 percent copper, seem to support this model. The interdendritic eutectic liquid in 38 percent alloys probably froze with supersaturated  $\alpha$  at the solidification front which constitutes these envelopes. A slow cooled plaster cast of 38 percent alloy showed very large envelopes of  $\alpha$  phase with almost no eutectic in between (Figure 52). However, the slow cooled eutectic alloys did not show large envelopes of  $\alpha$  around the eutectic dendrites, but coarse eutectic with irregular particles instead (Figure 54).

Solidification of 33 percent alloys in a flowing stream was studied in order to examine the above proposed mechanism. It was expected that if supersaturated  $\delta$  separates out from this liquid, then the liquid adjacent to the solidification front which is swept out by the flowing stream should have a higher copper content. Also, it was expected that a continuous supply of 33 percent liquid at the front would let this mechanism operate continuously and resultant structure might give a good support for the proposal. The results of the chemical analysis of this experiment for all the alloys are presented in Table IX. The variation in chemical composition is quite haphazard probably because of turbulence during the pours and also the overlapping of one solid layer over another. The composition of the 33 percent liquid seems to decrease instead of expected increase on pouring.

A vertical section along the pour direction (Figure 52) shows some primary dendrites and eutectic colonies. The eutectic colonies appear to grow upstream like dendrites and columnar<sup>31</sup> grains in other alloys. This indicates that colonies definitely grow with rejection of some species and preferential growth occurs in the direction where these are removed

continuously. An indirect outcome of this experiment was the comparison of fluidity of the three alloys. The fluidity varied inversely with the freezing range, the 33 percent alloy was most fluid and 24 percent the least as predicted elsewhere<sup>32</sup>.

Considering the mechanism proposed in this work for the solidification of eutectics, these experimental observations do not offer a very strong support to it. It has been indicated in the theory section that continued operation of this mechanism will result in a tremendous build up of copper concentration in liquid and also necessitate a large amount of  $\theta$  in the final structure. Therefore, it appears that this mechanism if at all operates, does so in the initial stages of freezing and then gives way to a different mechanism in the later stages. This could be the reason why we do not get large envelopes of  $\alpha$  around slow cooled eutectic colonies (Figure 54).

Figure 54, a section from the plaster cast eutectic, shows another interesting feature that the eutectic colony running across has a long plate of  $\theta$  near its axis all along its length, to which are attached all other lamella of  $\alpha$  and  $\text{CuAl}_2$ . No such observation has been reported before in

literature, to the authors knowledge, in an aluminum-copper eutectic structure. Figure 55, a view of the same colony at a higher magnification shows a discontinuity in the main stem and also slight thinning of side lamella at the point where they are attached to this main plate. Interdendritic eutectic in the slow cooled plaster cast ingots of 24 percent and 38 percent alloys also showed similar eutectic structure (Figures 56, 57, and 58). No such structure was observed in the faster frozen samples of either of these alloys.

It is obvious that this structure is not produced by simultaneous growth of nuclei of the two phases placed side by side. It appears that at slower freezing rates the eutectic grew as a anomalous eutectic and the nucleation and growth of the two phases was not so well coupled. The long platelet of  $\theta$  phase probably grew without nucleating any  $\alpha$ . Only when the  $\theta$  side branches started forming the supersaturation rose high enough for nucleation of  $\alpha$  phase and then the coupled growth resulted in lamellar structure.

A careful examination of Figure 52, in the light of this mechanism appears to lead to an explanation of envelopes

of  $\theta$  phase. The picture shows very little amount of  $\text{CuAl}_2$  present as long plates in between thick  $\text{CuAl}_2$  dendrites. It appears that after the formation of primary  $\text{CuAl}_2$  dendrites, the interdendritic eutectic liquid started freezing by deposition of  $\theta$  on the primary dendrites themselves. This divorcement of the eutectic caused a depletion of adjacent liquid in copper and brought its composition nearer to  $\alpha$ . But before the process could be completed, nucleation of  $\text{CuAl}_2$  occurred in the liquid away from the dendrites. This  $\text{CuAl}_2$  could lead to the formation of a very small amount of eutectic as the surrounding liquid was already depleted in copper, hence, giving rise to an envelope of  $\alpha$  around primary  $\theta$  particles.

Similar mechanism appears to be responsible for the continuous boundary of  $\text{CuAl}_2$  around  $\alpha$  particles of 24 percent alloy (Figure 58). However, in this case the envelope of  $\theta$  is very thin, whereas it should have been larger from the considerations of composition difference.



## VI. CONCLUSIONS

1. The dendrite spacing varies linearly with square root of freezing time even at very high solute concentrations, irrespective of the fact whether solute is rejected or consumed at the solidifying interface. The above behaviour is in accordance with the theory developed for growth of rod shaped dendrites.
2. Theoretical considerations show that solidification of a dendrite is effected by the presence of neighboring dendrites at very early stages of solidification process, but only after the primary dendrite spacing is established.
3. The tendency of side branching increases with the solute content, and its morphology cannot be predicted on purely crystallographic considerations. With increasing freezing rate the side branches appear to form along axes with larger fold symmetry (i.e., their number increases). However, the length of side branches decreases with increased freezing rates, and in low solute alloys these may completely vanish at very high freezing rates.
4. The increase of dendrite spacing with solute content is probably due to increase in super cooling of the liquid with the amount of solute to be rejected.

5. The lamellar eutectic between Al and  $\text{CuAl}_2$  arranges itself in typical dendritic form with side branches indicating that during eutectic solidification the plane front actually breaks down into dendritic protrusions. The colony spacing varies in the same fashion with the freezing rate as the dendrite spacing. The eutectic present between these colonies is coarse and irregular, and appears to form by a different mechanism.
6. The formation of eutectic colonies appears to be accompanied by rejection of certain species and they grow preferably in the direction where there is continuous supply of fresh liquid.
7. The presence of envelope of  $\alpha$  phase around eutectic colonies and  $\text{CuAl}_2$  dendrites leads to the suspicion that probably during eutectic solidification only one phase deposits in a supersaturated form and the second precipitates from this. This seemed to offer an identification of species rejected during the colony growth (if supersaturated  $\alpha$  separates, copper will be continuously rejected), and also an explanation of close similarity between colonies and dendrites.
8. Both the theoretical arguments and experimental observations indicate that this mechanism probably operates only in the very early stages of solidification and gives way to some other mode during later stages of growth.

9. The  $\alpha$  -  $\text{CuAl}_2$  eutectic behaves somewhat like a anomalous eutectic at slow growth rates, having a long platelet of  $\text{CuAl}_2$  along the length of the colony with lamellar eutectic on both sides of it. It appears that simultaneous growth of the two phases occurred only after a dendrite of  $\text{CuAl}_2$  had formed.
10. The presence of  $\alpha$  envelope around  $\text{CuAl}_2$  dendrites appears to be an outcome of eutectic divorcement.
11. The properties and mode of occurrence of dendritic particles in an alloy can radically effect the macroscopic properties of a casting even if the interdendritic liquid remains the same.
12. Fluidity of aluminum-copper alloys varies inversely with the freezing range.

## VII. SUGGESTIONS FOR FURTHER WORK

1. More systematic investigations should be performed to determine the dependence of dendrite spacing on solute content and the freezing range. Suitable systems should be selected which clearly bring about the difference in the role of these two parameters.
2. Direct experimental observations on supercooling in alloys are necessary to establish its dependence on solute content indicated by the present work. Also nucleation theories should be developed to explain this relationship.
3. Crystallography of side branching in dendrites needs investigation and its dependence of solute content and freezing rate appears to be an important aspect of dendritic growth. Studies of  $\text{CuAl}_2$  dendrites should be continued because it appears to be an interesting system due to its regularity and unique side branching characteristics.
4. Mathematical theories taking into account interactions of initial dendrites should be developed to predict at what stage of solidification side branching occurs, and its experimental confirmation based on relative thickness of side branches.

5. The present concepts of eutectic solidification do not appear to be satisfactory in explaining all the features of the growth process. Further work with purer materials should be conducted attempting to interrupt the process at different stages and examining the characteristics of growth. Direct investigation of compositions by electron microprobe in different regions (of eutectic within and in between the colonies) appears to be a promising tool for understanding the mechanism of solidification.
6. The lamella found in eutectic structure show some unusual characteristics. Further work need be conducted with controlled solidification conditions using several sections in order the understand the three dimensional aspects of lamellar growth. Electron microscope studies<sup>16</sup> appear to be very helpful in actually understanding the details of lamellar arrangement and defect structures therein.
7. The unique structures obtained on slow solidification of eutectics indicate the important role of cooling rate in changing the character of a eutectic. Systematic studies should be conducted to investigate the role of freezing rate on the mechanism of eutectic formation.

## APPENDIX I

INTERACTIONS BETWEEN NEIGHBORING DENDRITES

We consider two solidifying dendrites,  $2r_0$  distance apart,  $r_s$  being the radius of the solid portion at any instant (Figure 6). The basic assumption we make here is that the shape of the concentration profile in liquid remains the same during the process. Thus the amount of material diffusing out of any interface is proportional to the volume of material surrounding it. Applying this to interfaces at  $r$  and  $r_s$ .

$$-g_s D_1 \cdot 2\pi r_s = \pi (r_0^2 - r_s^2)$$

(Equation 11)

$$-g D_1 \cdot 2\pi r = \pi (r_0^2 - r^2)$$

(Equation 12)

where:  $g = \frac{dc}{dr}$  gradient at radius  $r$ .

$g_s = \left. \frac{dc}{dr} \right|_{r=r_s}$  gradients at radius  $r_s$ .

From (11) and (12) we get:

$$\frac{(r_o^2 - r_s^2)}{r_s g_s} \cdot \frac{dc}{dr} = \frac{r_s^2 - r^2}{r}$$

(Equation 13)

This equation on integration leads to the result

$$C_o - C_L = r_s g_s \left[ \left( \frac{r_o^2}{r_o^2 - r_s^2} \right) \ln \frac{r_o}{r_s} - \frac{1}{2} \right]$$

(Equation 14)

Taking the material balance across the freezing interface:

$$(1-K) C_L \frac{dr_s}{d\theta} = -Dg_s$$

(Equation 15)

Evaluating  $\frac{dr_s}{d\theta}$  from the relationship  $\beta^2 = \frac{r_s^2}{4D\theta}$  and substituting the relation<sup>19</sup>  $f = \frac{r_o^2 - r_s^2}{r_o^2} = \left( \frac{C_o}{C_L} \right)^{1/1-K}$

(where f is fraction of liquid) in equation 15 we get:

$$r_s g_s = -2 (1-K) C_o \beta^2 \left( \frac{r_o^2}{r_o^2 - r_s^2} \right)^{1-K}$$

(Equation 16)

From equations 14 and 16:

$$C_L - C_0 = (1-K) C_0 \beta^2 \left[ \frac{1}{f} \ln \left( \frac{1}{1-f} \right) - 1 \right]$$

(Equation 17)

Previously we have derived the equation for a dendrite rejecting solute, in a infinite medium.

$$C_L - C_0 = (1-K) C_0 \beta^2 [E(1) \beta^2]$$

we have taken  $e^{-\beta^2} = 1$   
as  $\beta$  is a small number  
and  $C_0 \approx C_L$

(Equation 7A)

Comparing equations 7A and 17 it is obvious that a dendrite becomes aware of its neighbor at that value of  $f$  for which the functions in square brackets in the two equations become equal. A calculation using the value of  $\beta = 0.05$  obtained from Browns<sup>7</sup> observations shows that this happens when the value of  $f$  equals 0.9984, in other words, quite early during the process of solidification.



## APPENDIX II

MATHEMATICAL ANALYSIS OF THE PROPOSED MODEL  
OF EUTECTIC SOLIDIFICATION

Figure 10 represents the model of eutectic growth in which only  $\alpha$  phase is shown to be in contact with the liquid and  $(\alpha + \beta) - \alpha$  interface is shown following the  $\alpha + L$  interface. The solid lines represent the actual concentration gradients (assumed to be error function curves for convenience) in the solid and liquid and the dotted lines represent the extrapolations of these gradients. The solutions of the error function concentrations<sup>20</sup> gradients are given by following equations.

$$\text{In Liquid: } \frac{C''_s - C}{C''_s - C_o} = e^{-\text{erfc}^2 \frac{X}{2\sqrt{D''\theta}}}$$

(Equation 18)

$$\text{In Solid: } \frac{C - C'_s}{C'_o - C'_s} = e^{-\text{erfc}^2 \frac{X}{2\sqrt{D'\theta}}}$$

(Equation 19)

where:  $C$  = Concentration at distance  $X$  and time  $(\theta)$ .

$C''_s$  = Intersection of concentration gradient curve in liquid at  $X = 0$ .

$C'_s$  = Intersection of concentration gradient curve in solid at  $X = 0$ .

$C_o$  = Average concentration of liquid.

$C_e$  = Average concentration of eutectic solid  $\approx C_o$ .

$D'$  = Diffusion coefficient in solid.

$D''$  = Diffusion coefficient in liquid.

Assuming parabolic growth rate for both the interfaces, we define growth constants  $\alpha, \beta$  and  $\gamma$ .

$$x_1 = 2\alpha\sqrt{D'\theta} \quad (\text{Equation } \underline{20})$$

$$x_2 = 2\beta\sqrt{D'\theta} \quad (\text{Equation } \underline{21})$$

$$x_2 = 2\gamma\sqrt{D''\theta} \quad (\text{Equation } \underline{22})$$

and  $\frac{\gamma}{\beta} = \sqrt{D'/D''} \quad (\text{Equation } \underline{22A})$

Further in order to eliminate  $C''_s$  and  $C'_s$  we set following constants:

$$C_o - C'_s = A = \frac{C_2 - C_1}{\text{erf}\beta - \text{erf}\alpha}$$

(Equation 23)

$$C''_s - C_o = B = \frac{C_3 - C_o}{1 - \text{erf}\gamma}$$

(Equation 24)

Also we can write concentration gradients at the interfaces both in liquid and solid:

$$\left(\frac{\partial c}{\partial x}\right)_{s, X_1} = \frac{Ae^{-\alpha^2}}{\sqrt{\pi D^* \theta}}$$

(Equation 25)

$$\left(\frac{\partial c}{\partial x}\right)_{l, X_2} = \frac{Ae^{-\beta^2}}{\sqrt{\pi D'' \theta}}$$

(Equation 26)

$$\left(\frac{\partial c}{\partial x}\right)_{l, X_2} = \frac{e^{-\gamma^2}}{\sqrt{\pi D'' \theta}}$$

(Equation 27)

In the above equations on the left hand side first subscript refers to the phase the second to the interface.

Applying the first boundary condition that movement of interface I is governed by diffusion of copper to it:

$$(c_0 - c_1) \frac{dx_1}{d\theta} = D^* \left(\frac{\partial c}{\partial x}\right)_{s, X_1}$$

(Equation 28)

substituting the value of gradients from previous equations:

$$(C_e - C_L) \sqrt{\pi} = \frac{C_2 - C_1}{\alpha e^{\alpha^2} (\operatorname{erf} \beta - \operatorname{erf} \alpha)}$$

(Equation 29)

Applying the second boundary condition that movement of II is governed by diffusion both in liquid and in solid:

$$(C_3 - C_2) dx_2/d\theta = D' \left( \frac{\partial C}{\partial x} \right)_{1, X_2} - D'' \left( \frac{\partial C}{\partial x} \right)_{1, X_2}$$

(Equation 30)

substitution from previous equations leads to following results:

$$(C_3 - C_2) \sqrt{\pi} = \frac{C_2 - C_1}{\beta e^{\beta^2} (\operatorname{erf} \beta - \operatorname{erf} \alpha)} + \frac{C_3 - C_0}{\gamma e^{\gamma^2} (1 - \operatorname{erf} \gamma)}$$

(Equation 31)

Equations 29 and 31 were solved by trial and error for  $\alpha$  and  $\beta$  taking the value of  $r$  as 10 and undercooling  $.10^\circ\text{C}$ . The values of  $\beta$  and  $\alpha$  were found to be quite small ( $\beta = 4.9 \times 10^{-2}$  and  $\alpha = 4.9 \times 10^{-2}$ ), indicating that the rate of growth of such a front is very small. This implies that for a required growth rate a large number of such fronts would be needed and their number would increase with increased rate of heat extraction.

## VIII. TABLES AND ILLUSTRATIONS

TABLE I

## COMPOSITION OF ALUMINUM USED FOR ALLOY PREPARATION

---

|         |          |         |      |      |
|---------|----------|---------|------|------|
| Element | Aluminum | Silicon | Iron | Zinc |
| Percent | 99.72    | 0.12    | 0.14 | 0.02 |

---

TABLE II  
CALCULATIONS OF SOLIDIFICATION PARAMETER

Voltage - 10 Volts  
 Current - 350 Amps.  
 Power - 350 x 10 Watts  
       - 350 x 10 x .0569  $\frac{\text{B.T.U./min.}}{\text{Watts}}$   
       - 350 x 10 x .0569 x 60  $\frac{\text{B.T.U.}}{\text{hour}}$   
       - 11900  $\frac{\text{B.T.U.}}{\text{hour}}$

| No. | Speed of Arc                 |                    | Parameter          | Parameter |              |
|-----|------------------------------|--------------------|--------------------|-----------|--------------|
|     | High Scale Inches<br>Setting | Inches<br>per min. | Feet per<br>minute | $q/v$     | $\sqrt{q/v}$ |
| 1   | 150                          | 91.5               | 457.5              | 26        | 5.10         |
| 2   | 140                          | 83.5               | 417.5              | 28.4      | 5.35         |
| 3   | 130                          | 76.0               | 380.0              | 31.4      | 5.60         |
| 4   | 120                          | 68.0               | 340.0              | 35.0      | 5.92         |
| 5   | 110                          | 60.0               | 300.0              | 39.6      | 6.30         |
| 6   | 100                          | 52.25              | 262.25             | 45.20     | 6.73         |
| 7   | 90                           | 44.50              | 222.50             | 53.40     | 7.30         |
| 8   | 80                           | 36.50              | 182.50             | 65.10     | 8.09         |
| 9   | 70                           | 28.00              | 160.00             | 74.40     | 8.60         |
| 10  | 60                           | 21.00              | 105.00             | 113.00    | 10.60        |
| 11  | 50                           | 13.00              | 65.00              | 183.00    | 13.50        |
| 12  | 40                           | 5.00               | 25.00              | 475.00    | 21.80        |

TABLE III

VARIATION OF DENDRITE SPACING WITH SOLIDIFICATION  
PARAMETER FOR 24% COPPER ALLOY

| No. | Solidification Parameter $\sqrt{q/v}$ | Dendrite Spacing<br>in Microns |
|-----|---------------------------------------|--------------------------------|
| 1   | 5.10                                  | 10.4                           |
| 2   | 5.35                                  | 11.0                           |
| 3   | 5.60                                  | 12.10                          |
| 4   | 5.92                                  | 15.00                          |
| 5   | 6.30                                  | 14.52                          |
| 6   | 6.73                                  | 14.50                          |
| 7   | 7.30                                  | 16.2                           |
| 8   | 8.09                                  | 17.49                          |
| 9   | 8.60                                  | 18.50                          |
| 10  | 10.60                                 | 24.60                          |
| 11  | 13.50                                 | 30.00                          |
| 12  | 21.80                                 | 49.00                          |

TABLE IV

VARIATION OF DENDRITE SPACING WITH COPPER CONTENT  
AT SOLIDIFICATION PARAMETER VALUE  $\sqrt{q/v} = 10$

| No. | Percentage Copper | Dendritic Spacing in<br>Microns |
|-----|-------------------|---------------------------------|
| 1   | 0.98%             | 4.1* micron                     |
| 2   | 0.44%             | 6.8* micron                     |
| 3   | 24.00%            | 22.25                           |
| 4   | 38.00%            | 14.5                            |

\* Data from Browns<sup>7</sup> Work.

TABLE V

VARIATION OF GROWTH CONSTANT ( $\beta$ ) WITH COPPER CONTENT

| No. | Percent Copper | Values |
|-----|----------------|--------|
| 1   | 1              | .037   |
| 2   | 4.5            | .050   |
| 3   | 24             | .153   |

TABLE VI

VARIATION OF DENDRITE SPACING WITH SOLIDIFICATION RATE FOR 24% COPPER ALLOY

| No. | Solidification Parameter $\sqrt{q/v}$ | Dendritic Spacing in Microns |
|-----|---------------------------------------|------------------------------|
| 1   | 5.10                                  | 7.00                         |
| 2   | 5.35                                  | 7.25                         |
| 3   | 5.60                                  | 8.90                         |
| 4   | 5.92                                  | 8.02                         |
| 5   | 6.30                                  | 9.98                         |
| 6   | 6.73                                  | 10.20                        |
| 7   | 7.30                                  | 10.50                        |
| 8   | 8.09                                  | 10.80                        |
| 9   | 8.60                                  | 11.20                        |
| 10  | 10.60                                 | 15.25                        |
| 11  | 13.50                                 | 20.00                        |
| 12  | 21.80                                 | 22.25                        |



TABLE VII

VARIATION OF COLONY SPACING WITH SOLIDIFICATION RATE IN  
ALUMINUM COPPER EUTECTIC ALLOY

| No. | Solidification Parameter $\sqrt{q/v}$ | Colony Spacing in<br>Microns |
|-----|---------------------------------------|------------------------------|
| 1   | 5.10                                  | 6.1                          |
| 2   | 5.35                                  | 5.3                          |
| 3   | 5.60                                  | 6.0                          |
| 4   | 5.92                                  | 6.75                         |
| 5   | 6.30                                  | 6.50                         |
| 6   | 6.73                                  | 7.3                          |
| 7   | 7.30                                  | 7.45                         |
| 8   | 8.09                                  | 7.85                         |
| 9   | 8.60                                  | 9.70                         |
| 10  | 10.60                                 | 10.90                        |
| 11  | 13.50                                 | 13.90                        |
| 12  | 21.80                                 | 19.20                        |

TABLE VIII

VARIATION OF INTERLAMELLAR SPACING WITH SOLIDIFICATION RATE  
IN ALUMINUM COPPER EUTECTIC  
ALLOY

| No. | $\sqrt{v}/v$ | Interlamellar Spacing x 10 <sup>-1</sup> Microns |
|-----|--------------|--|
| 1   | 5.10         |  |
| 2   | 5.35         | Unresolvable at 2500X                            |
| 3   | 5.60         |  |
| 4   | 5.92         |  |
| 5   | 6.32         | 3.2  |
| 6   | 6.73         | 3.35   |
| 7   | 7.30         | 3.5  |
| 8   | 8.03         | 3.62   |
| 9   | 8.60         | 4.176  |
| 10  | 10.60        | 4.268  |
| 11  | 13.50        | 4.500  |
| 12  | 21.80        | 5.40   |

TABLE IX

## RESULTS\* OF SOLIDIFICATION STUDIES IN FLOWING STREAM

| No. | Nominal Alloy Composition | Composition of Liquid Poured | Compositions Along the Length of Frozen Strip (12" Intervals) |       |       |       |       |       |       |        | Average Solid Composition | Composition of Remaining Liquid |
|-----|---------------------------|------------------------------|---|-------|-------|-------|-------|-------|-------|--------|---------------------------|---------------------------------|
| I   | 24                        | 24.68                        | 24.25   | 24.27 | 24.52 | 24.19 | 24.73 | 24.51 | 24.66 | 24.44  | 24.42                     |                                 |
|     |                           | 24.42                        | 24.62   | 24.74 | 29.72 | 23.96 | 24.36 | 24.34 | 23.81 | 24.36  | N.A.                      |                                 |
| II  | 33                        | 32.60                        | 32.49   | 32.11 | 32.09 | 32.34 | 32.44 |       |       | 32.294 | 32.63                     |                                 |
|     |                           | 32.63                        | 32.54   | 32.06 | 32.11 | 32.27 | 31.61 | 31.78 |       | 32.06  | 32.4                      |                                 |
|     |                           | 32.4 ± 0.2                   | 32.47   | 32.64 | 32.51 | 32.16 | 32.41 | 32.04 |       | 32.38  | N.A.                      |                                 |
| III | 38                        | 38.75                        | 38.67   | 38.43 | 39.41 | 39.17 | 38.22 | 38.84 |       | 38.87  | 38.67                     |                                 |
|     |                           | 38.67                        | 39.36   | 39.06 | 39.29 | 38.29 | 37.97 | 37.68 | 37.74 | 38.48  | 38.87                     |                                 |
|     |                           | 38.87                        | 37.18   | 38.05 |       |       |       |       |       | 37.61  |                           |                                 |

\* All Numbers Represent Percentage of Copper

Figure 1: Schematic Phase diagram for the case  $K < 1$  representing the concentrations of liquid and solid in equilibrium.

Figure 2: Schematic representation of solute concentration profile near a Solid-Liquid interface.

Figure 3: Representation of the relation between actual temperature gradient and liquidous temperature corresponding to solute concentration build up in Figure 2.

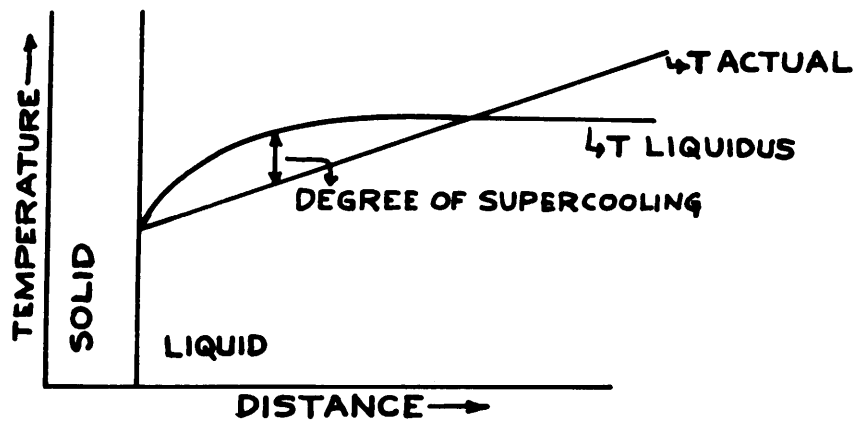
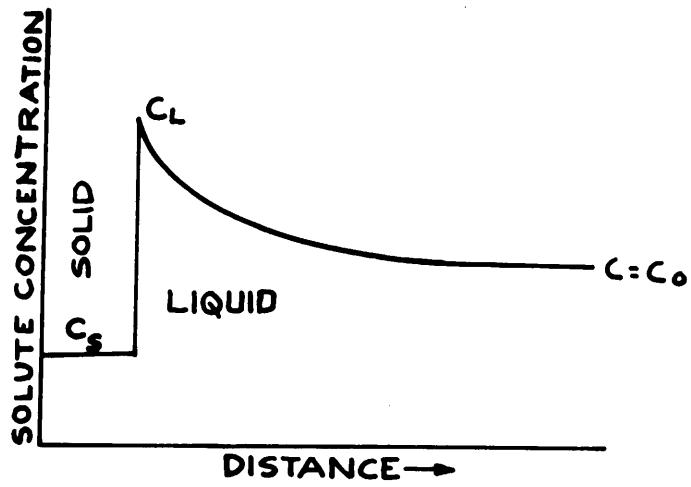
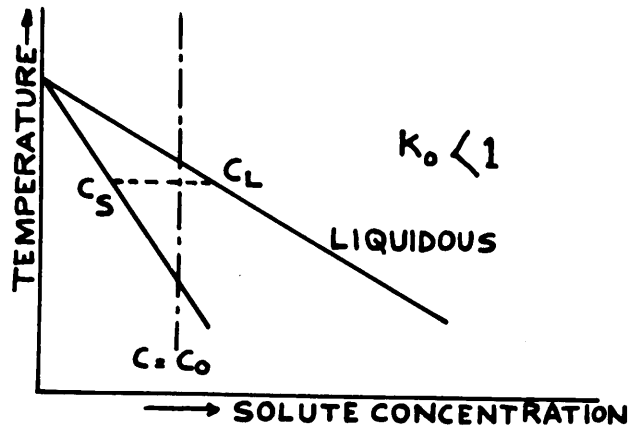


Figure 4: Solute concentration profile in the liquid surrounding a growing rod shaped dendrite.

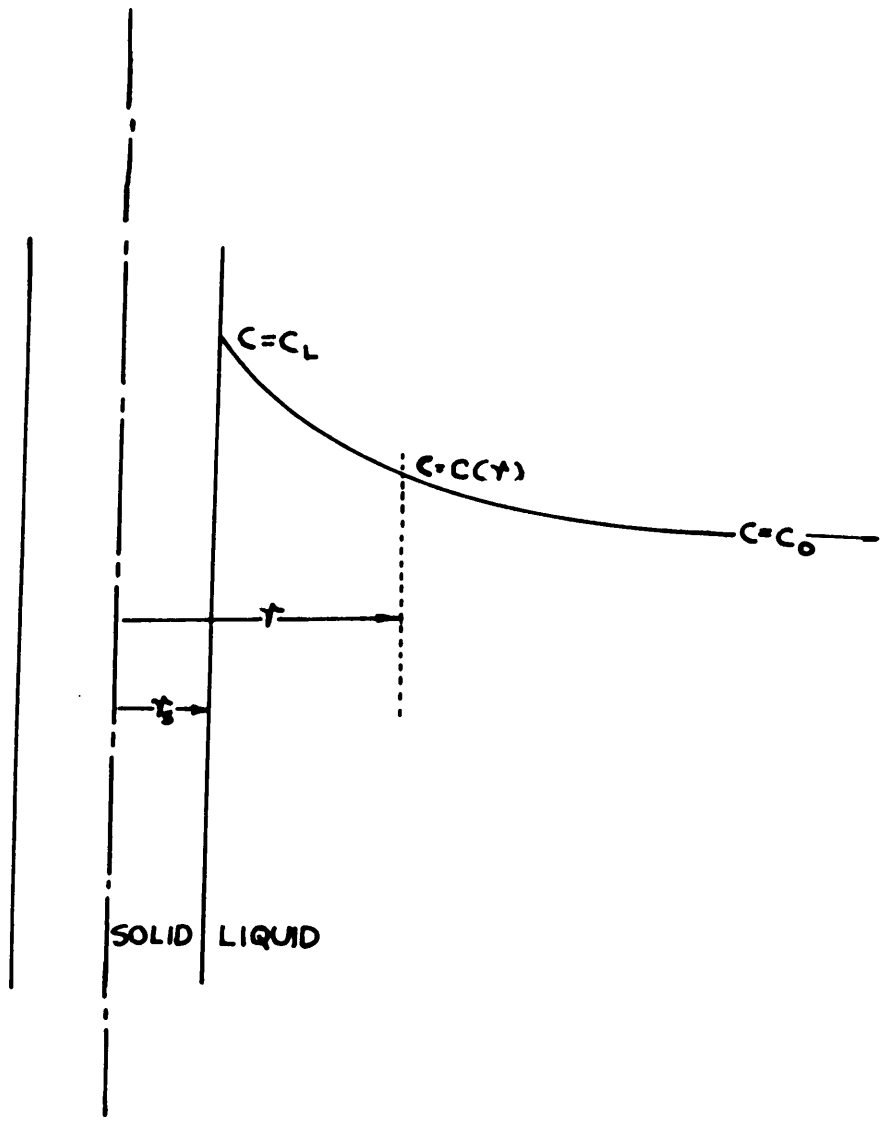


Figure 5: Relation between growth constant ( $\beta$ ) and supercooling in liquid for a aluminum-copper alloy with 4.5 percent copper.



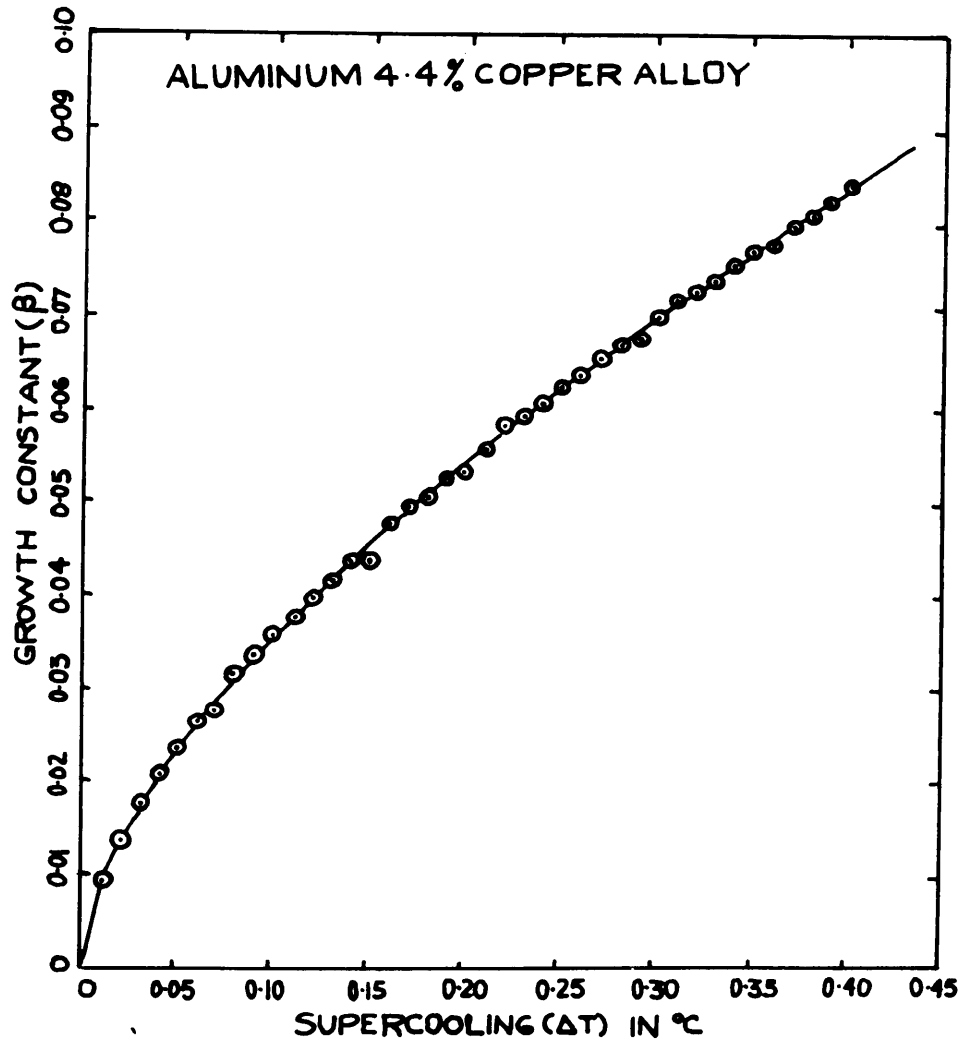


Figure 6: Representation of two neighboring dendrites during growth process. The sectioned area represents the solid rod shaped dendrites which are surrounded by liquid on all sides.

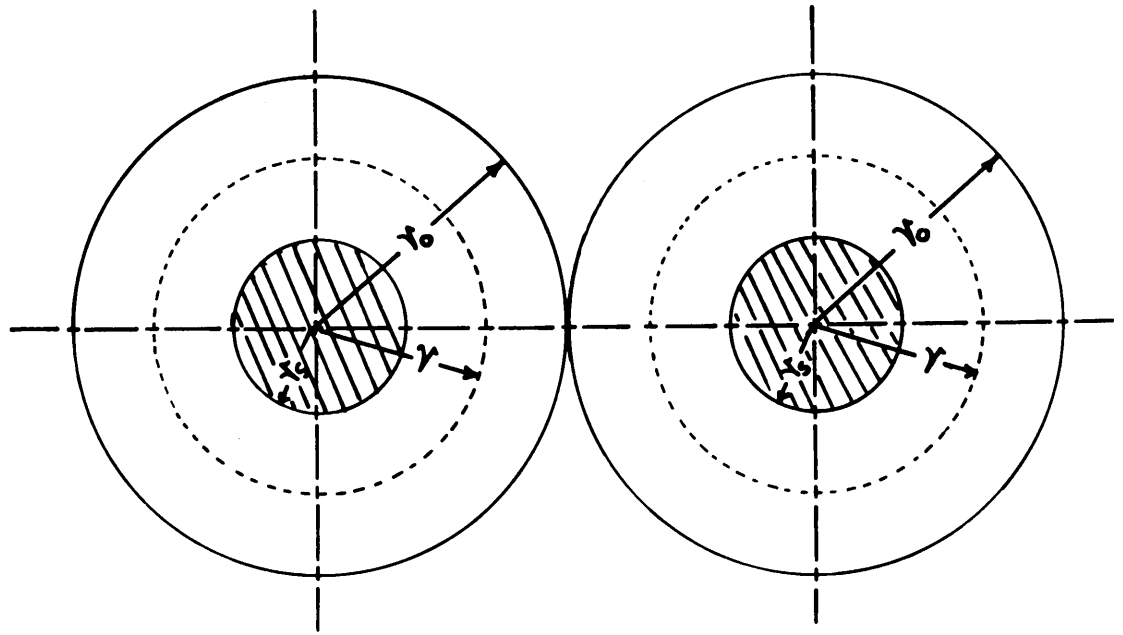


Figure 7: Copper rich end of the aluminum-copper phase diagram. Dotted lines represent the extensions of actual phase boundaries followed in case of supercooling.

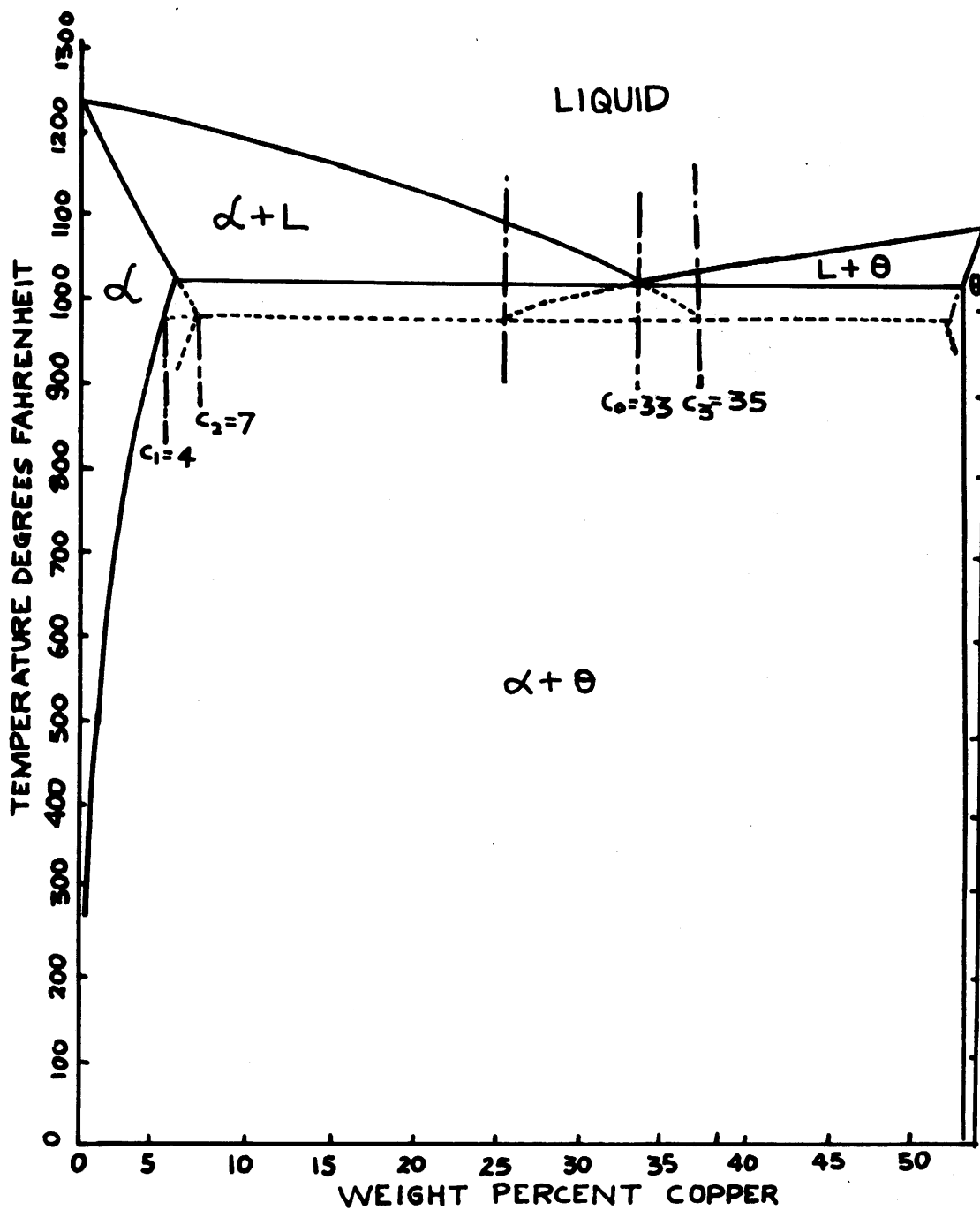


Figure 8:; Representation of the lamella of  $\alpha$  and  $\text{CuAl}_2$  placed side by side during eutectic growth. The numbers represent the approximate copper concentrations taken from Figure 7.

Figure 9: Shows the overlapping of  $\alpha$  phase around  $\theta$  lamella because of differential growth rates of the interfaces in Figure 8.

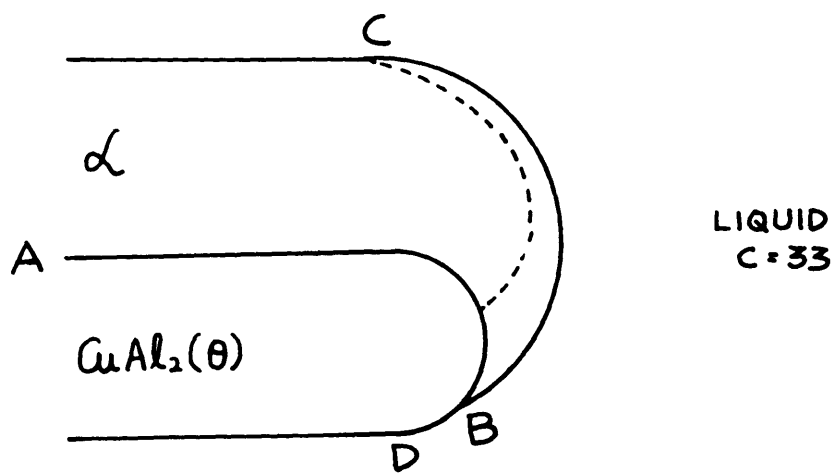
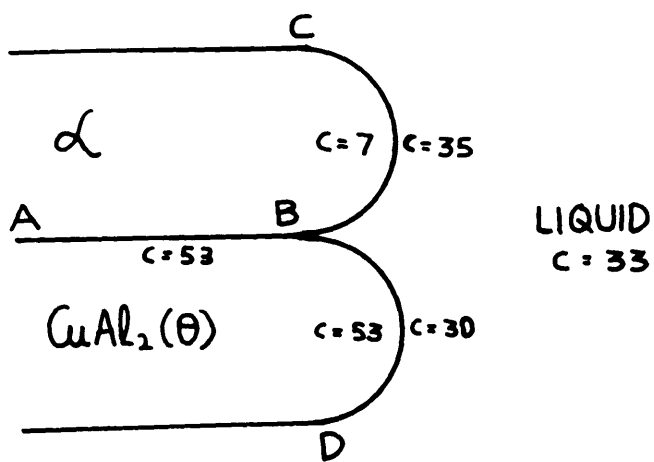


Figure 10: Representation of the proposed model for eutectic growth, showing  $\alpha$ - $\alpha+\beta$  interface following the  $\alpha$ -liquid interface. The solid lines represent the actual concentration gradients in liquid and solid. The dotted lines are just the extensions of these concentration profiles.



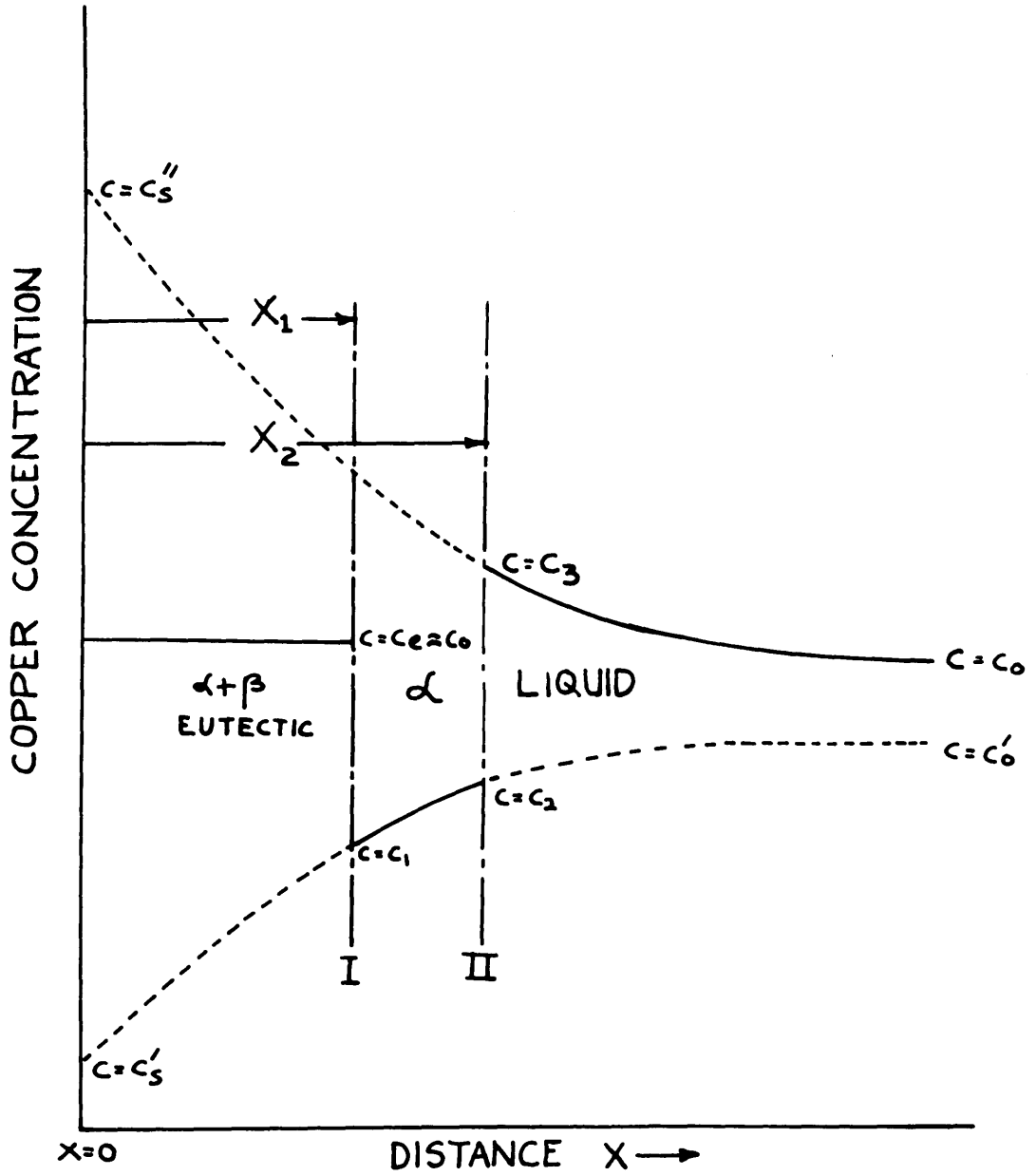


Figure 11: Diagram of the permanent tungsten electrode inert gas equipment used to produce arc deposits.

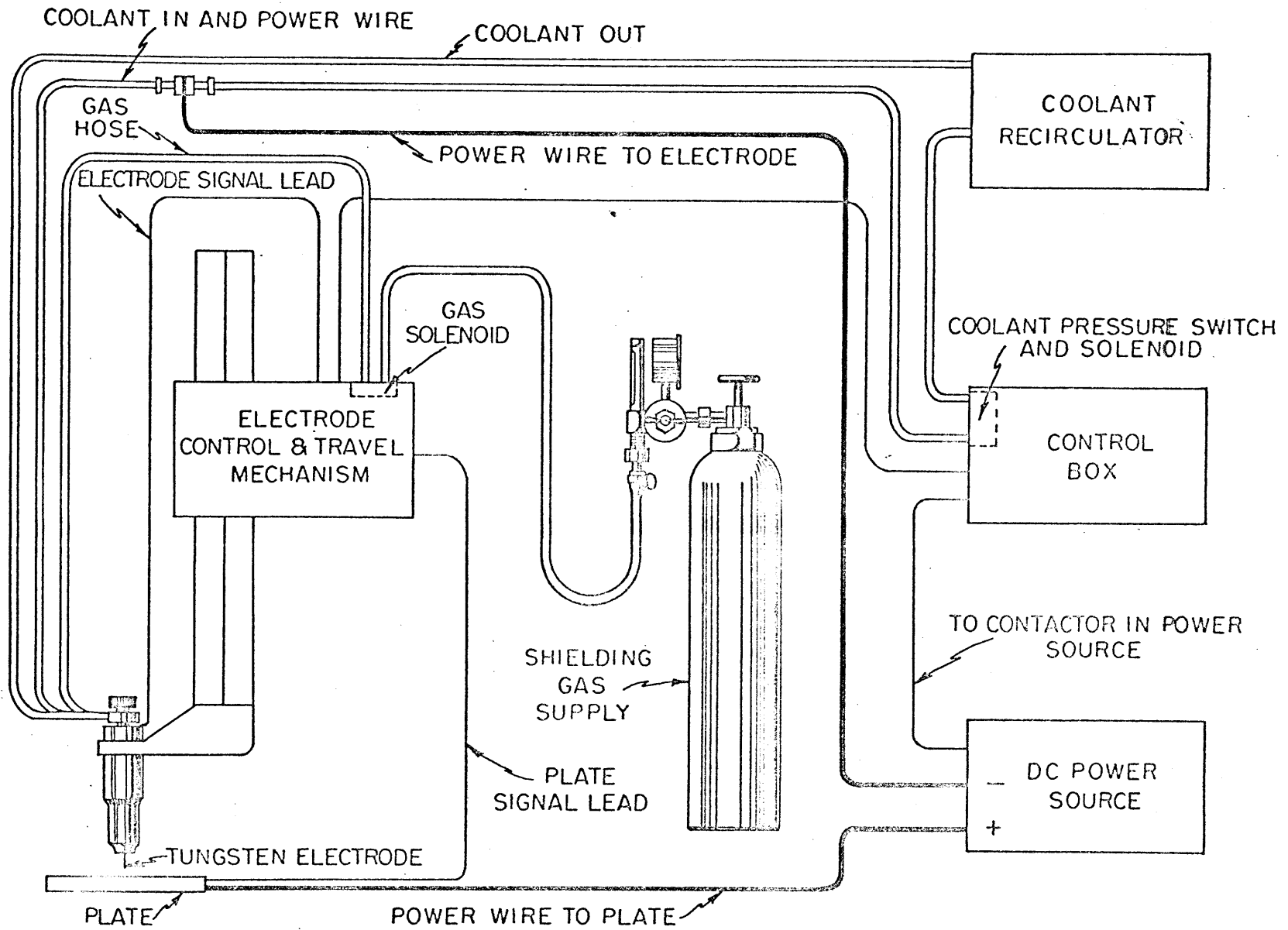


Figure 12: Schematic diagram showing the position of arc deposits on the cast plates, also indicating the planes along which specimens for metallographic examination were taken.

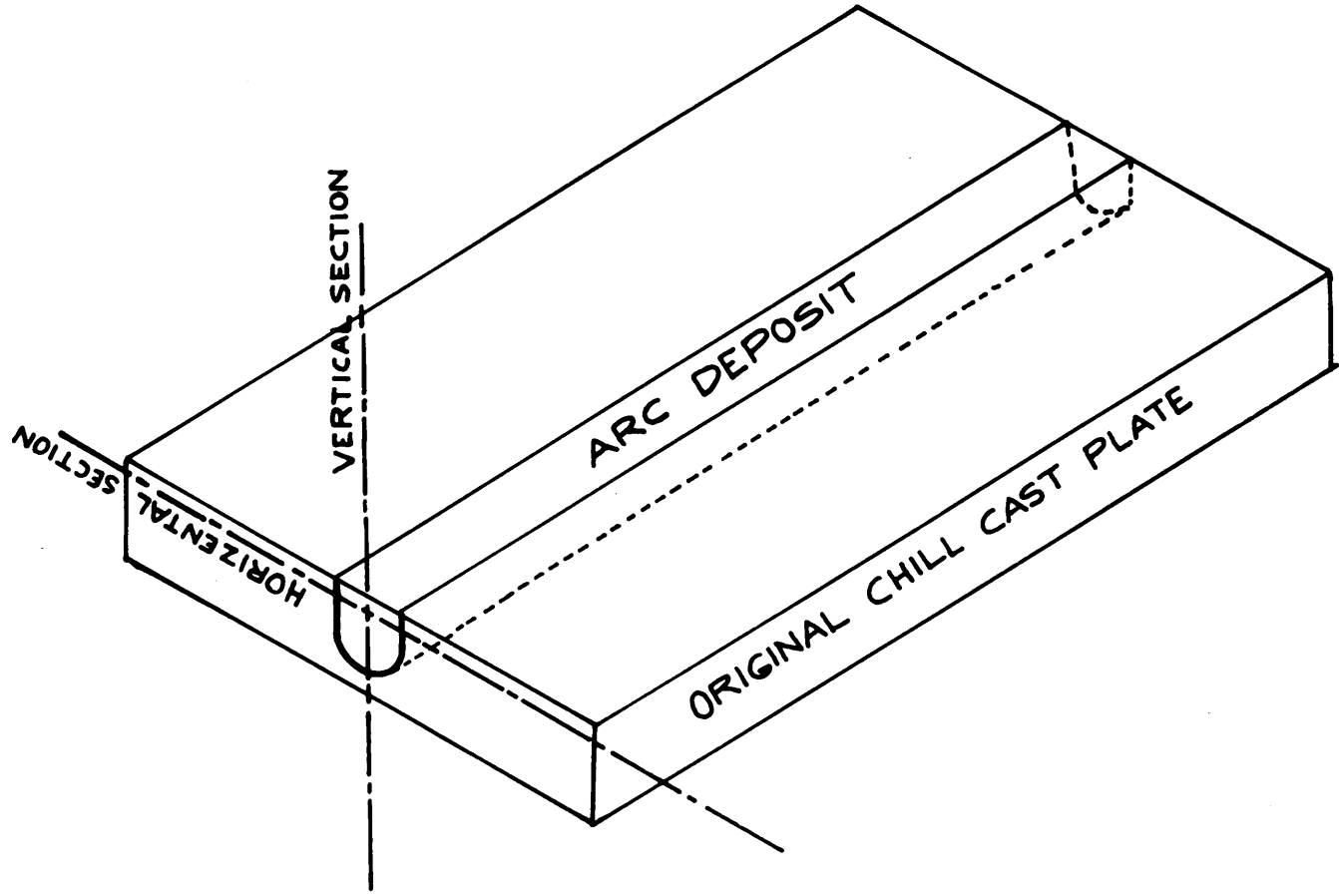


Figure 13: Diagram showing the chilling trough used for studying the solidification behaviour in a flowing stream.

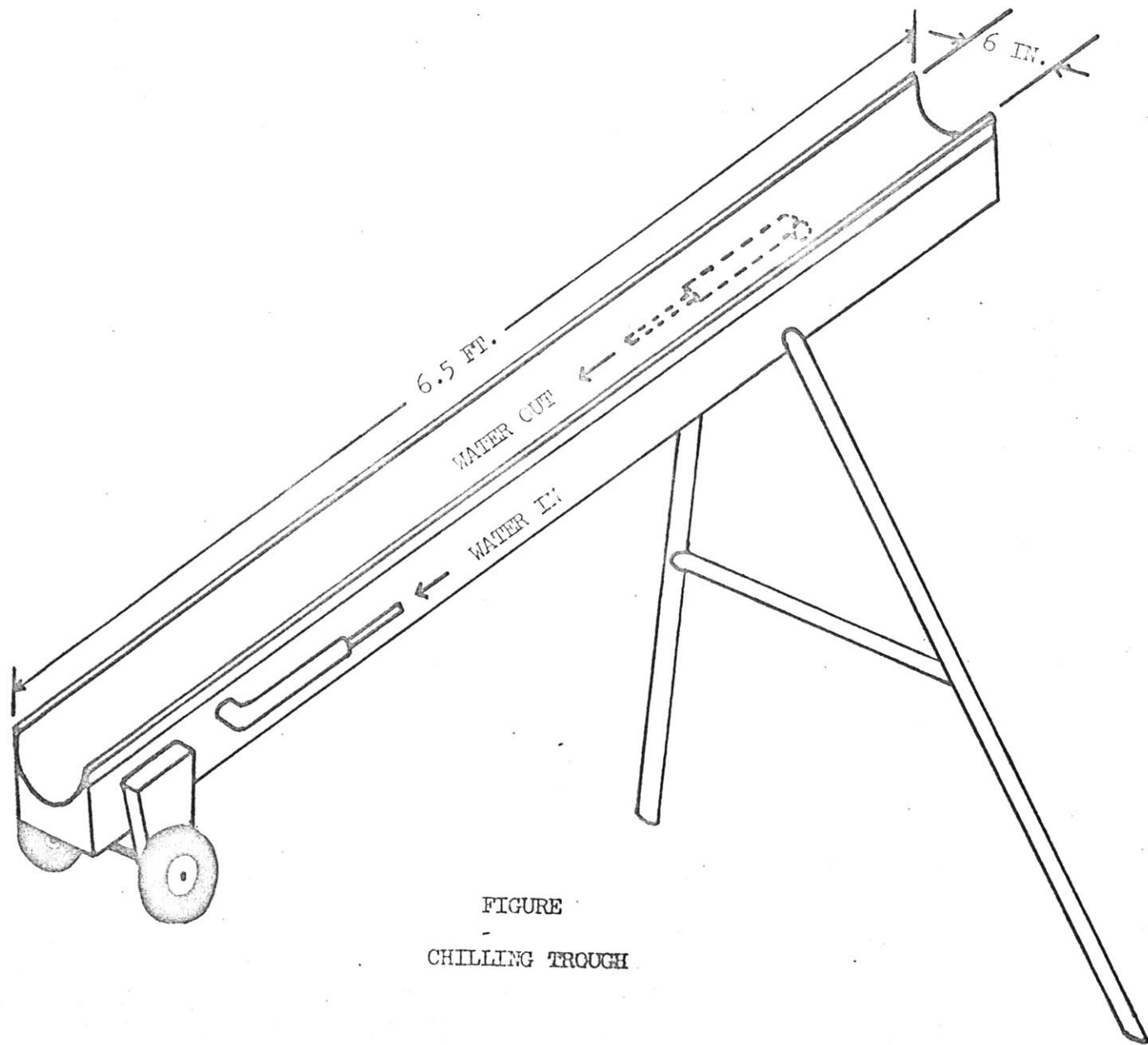


FIGURE  
CHILLING TROUGH

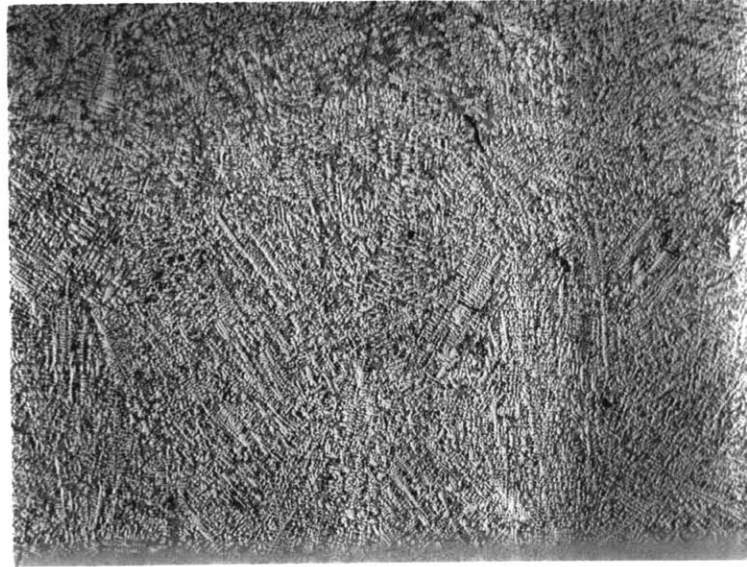


Figure 14: Vertical section through cast plate of 24 percent copper alloy showing dendritic nature of the plate. X50 Etch  $\text{HNO}_3$

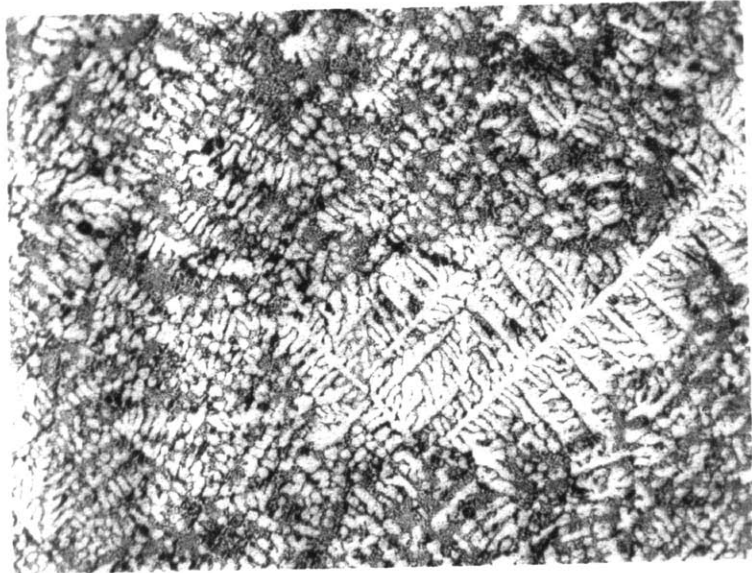


Figure 15: Vertical section through 24 percent copper alloy plate showing typical  $\alpha$  dendrites. X50 Etch  $\text{HNO}_3$



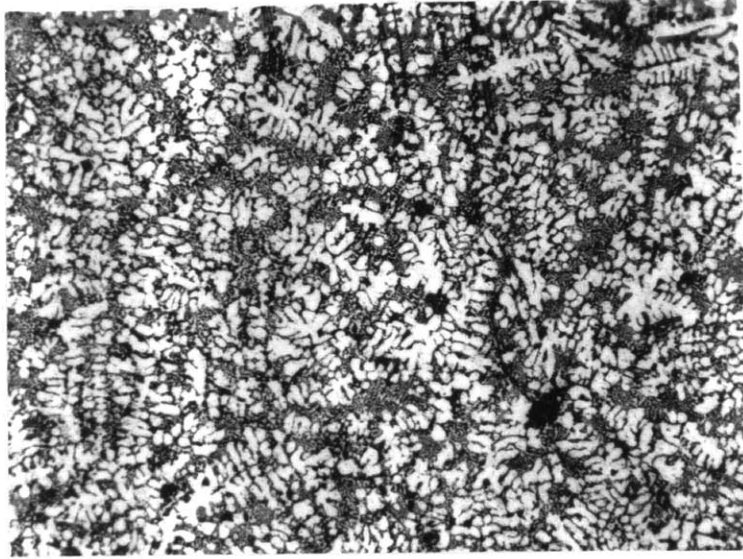


Figure 16: Horizontal section through 24 percent alloy plate showing transverse section of  $\alpha$  dendrites. X50 Etch  $\text{HNO}_3$

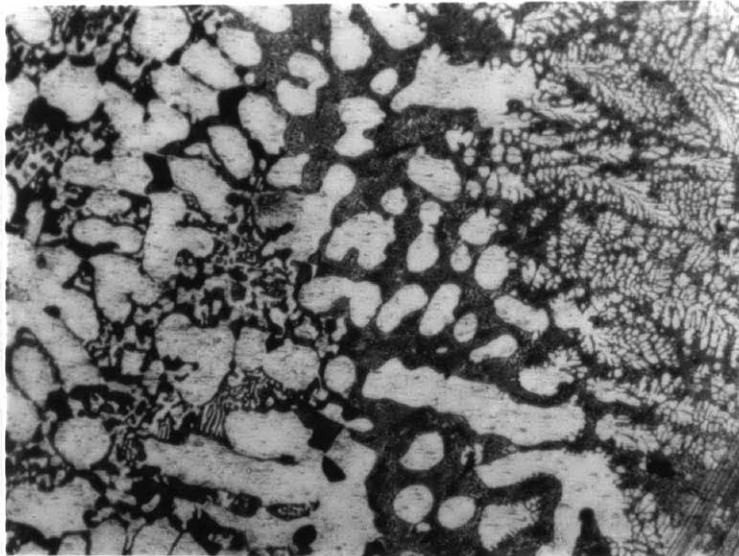


Figure 17: Vertical section of arc deposit interface in 24 percent copper alloy showing original plate structure, transition zone and arc deposit structure from left to right. X200 Etch  $\text{HNO}_3$

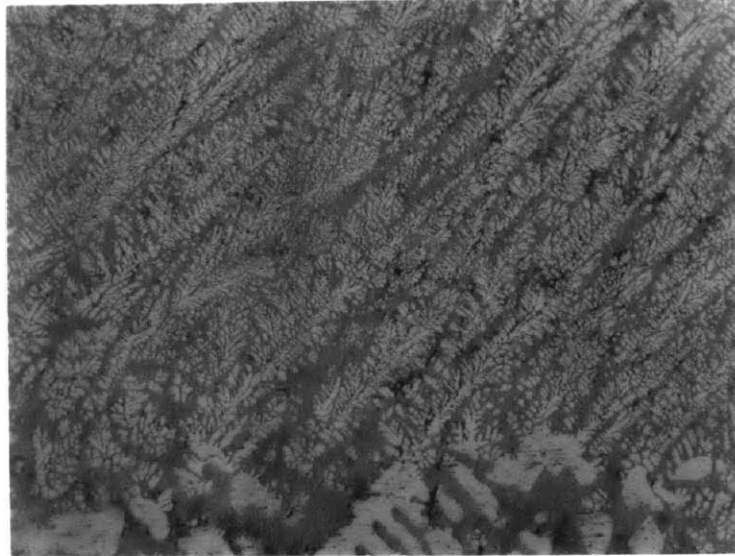


Figure 18: Vertical section of arc deposit in 24 percent copper alloy showing parallel dendrites of  $\alpha$  nucleated at the interface. X150 Etch  $\text{HNO}_3$



Figure 19: Horizontal section of arc deposit far from interface showing long  $\alpha$  dendrites along the length of the weld. X 500 Etch  $\text{HNO}_3$

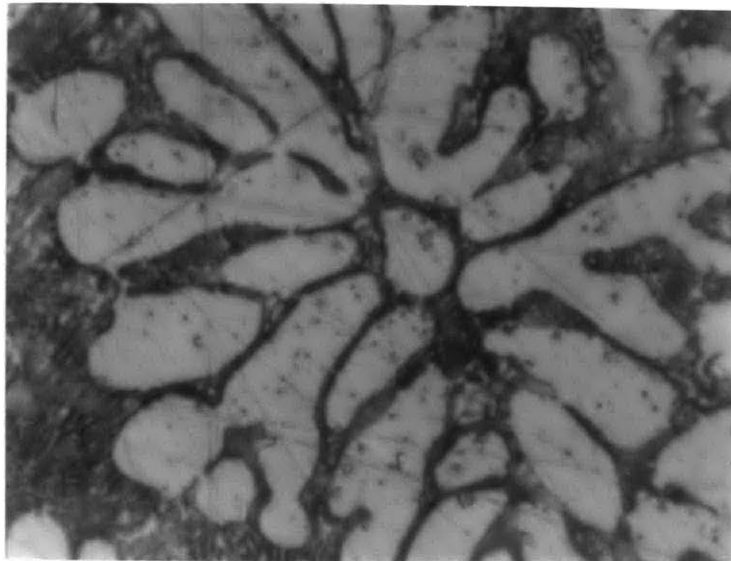


Figure 20: A transverse section across an  $\alpha$  dendrite in arc deposit of 24 percent copper alloy showing the arrangement of side branches around central stem.  
X 2500 Etch  $\text{HNO}_3$

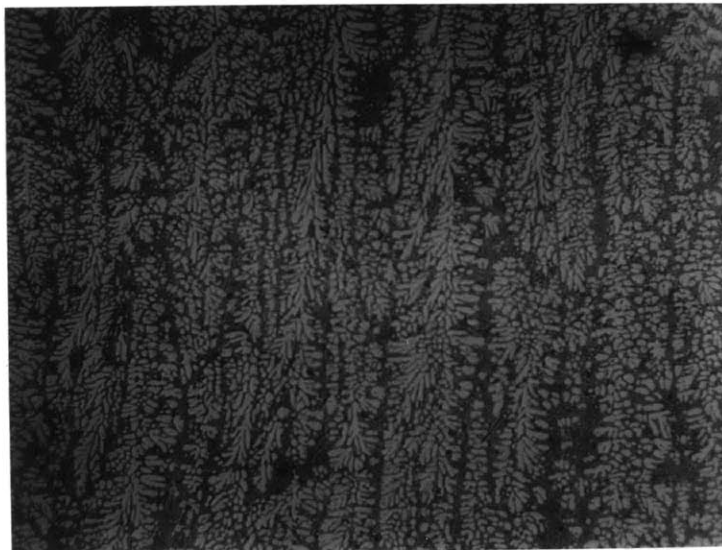
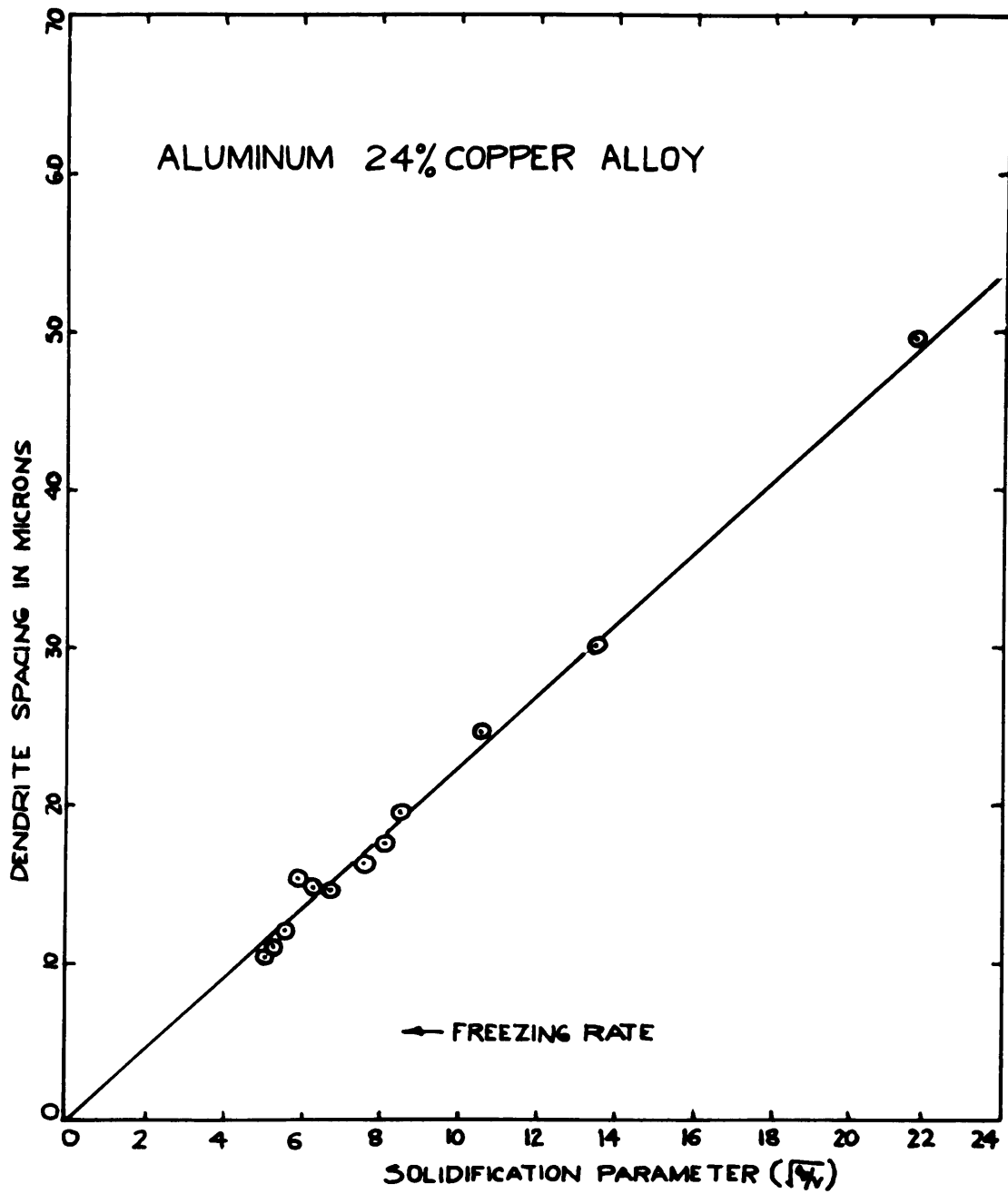


Figure 21: Vertical section through slowly cooled arc deposit in 24 percent copper alloy showing parallel dendrites of  $\alpha$ .  
X 250 Etch  $\text{HNO}_3$

Figure 22: Relationship between dendrite spacing and freezing rate in 24 percent copper alloy arc deposits.



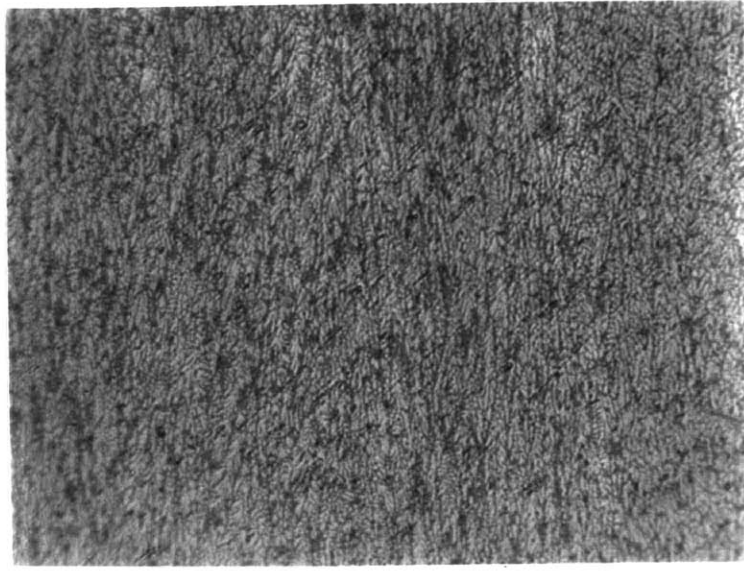


Figure 23: Vertical section through arc deposit in 24 percent copper alloy at  $\sqrt{q/v} = 5$  showing finely spaced dendrites. X500 Etch  $\text{HNO}_3$

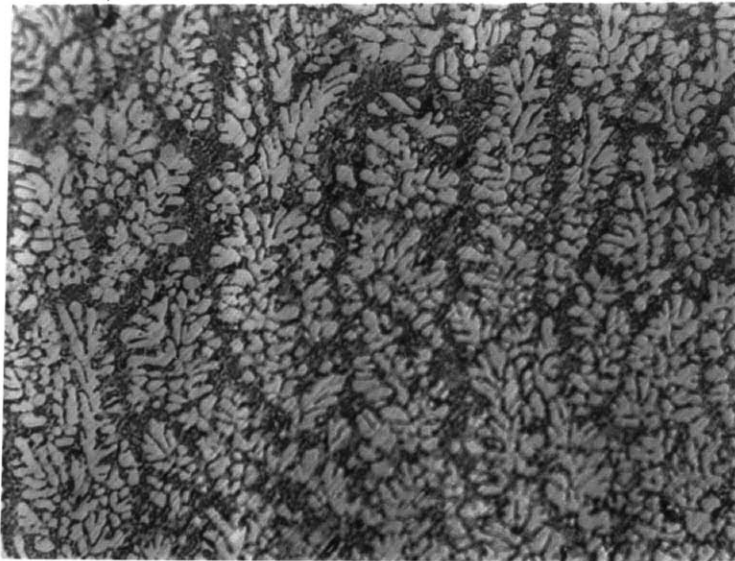
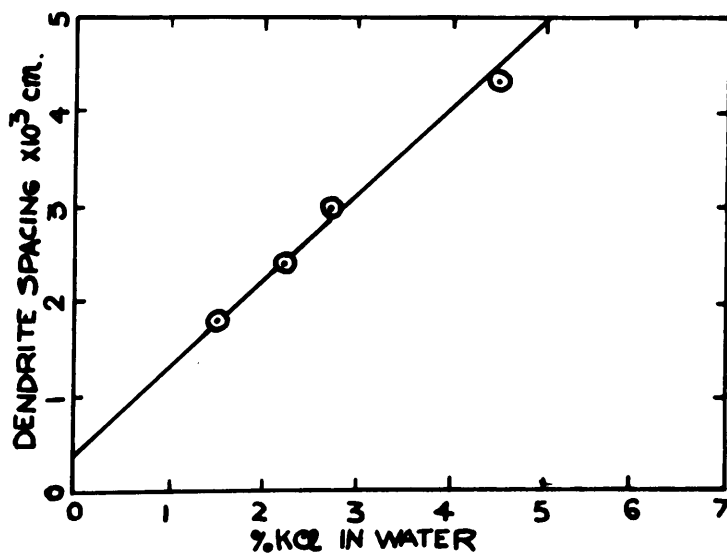
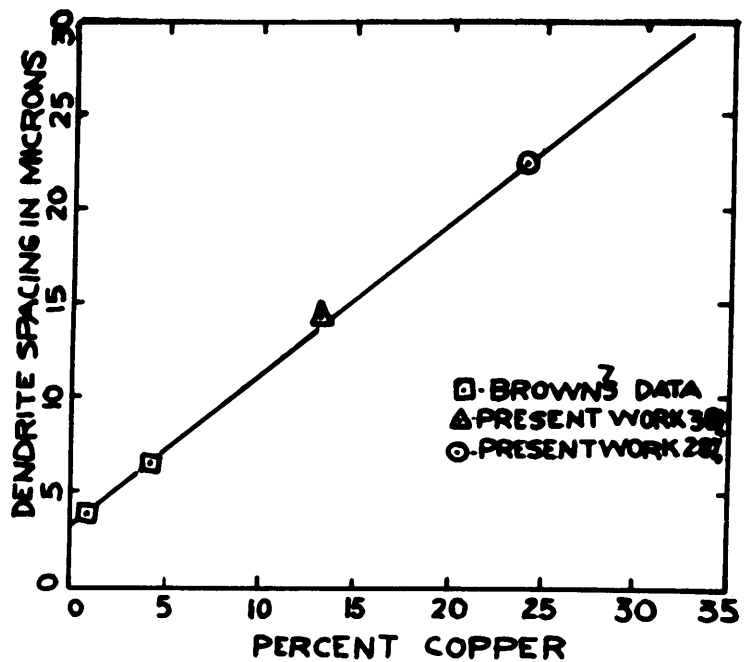


Figure 24: Vertical section through arc deposit of 24 percent copper alloy at  $\sqrt{q/v} = 21$  showing larger dendrite spacing compared to Figure 23. X500 Etch  $\text{HNO}_3$

Figure 25: Relationship between dendrite spacing and copper content in aluminum-copper alloys for freezing rates corresponding to solidification parameter.  $\sqrt{q/v} = 10$ .

figure 26: Diagram showing variation in spacing of ice dendrites with KCl content in water at a freezing time of one minute. (Data from reference 8).





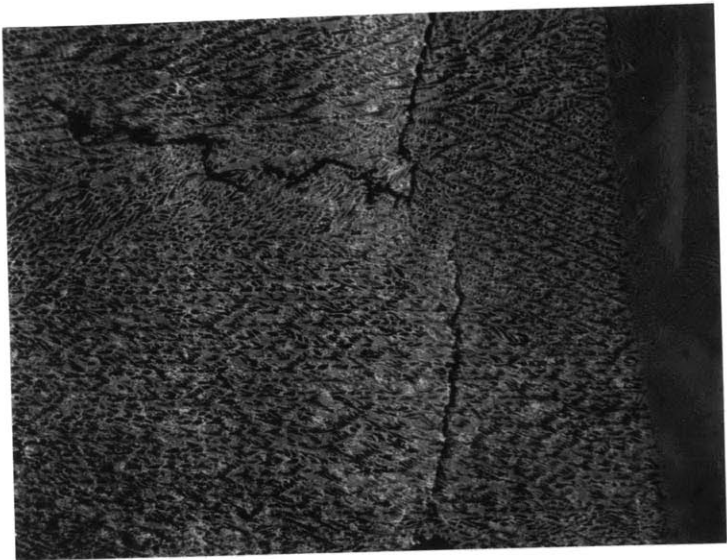


Figure 27: Vertical section of 38 percent copper alloy chilled plate showing parallel dendrites grown perpendicular to chill surface. Fine structure on the right is section through arc deposit in the same plate. X 13 Etch  $\text{HNO}_3$



Figure 28: Horizontal section through 38 percent copper alloy chilled cast plate showing three fold symmetry in arrangement of side branches in  $\text{CuAl}_2$  dendrites. X 50 Etch  $\text{HNO}_3$

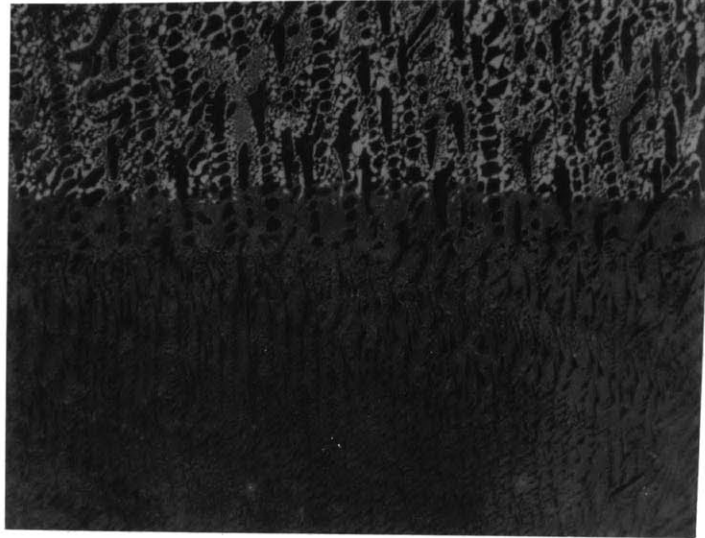


Figure 29: Vertical section near arc deposit interface in 38 percent copper alloy plate showing on top original chilled cast plate, the transition zone and then fine structure in the arc deposited region. X50 Etch  $\text{HNO}_3$

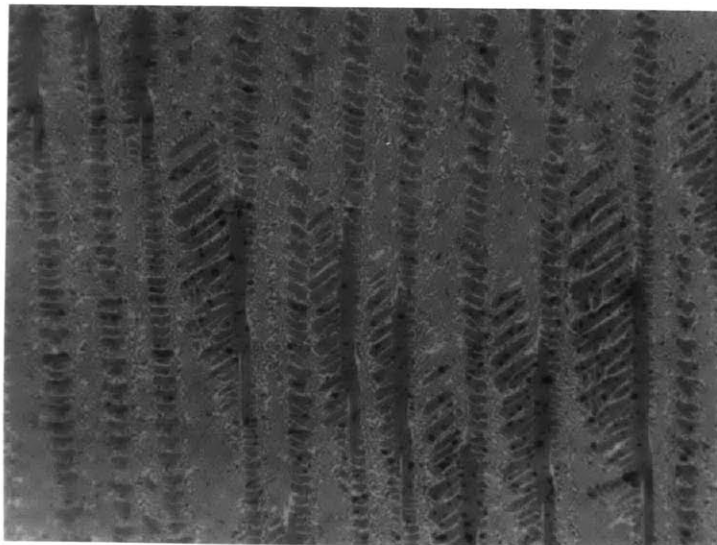


Figure 30: Vertical section of arc deposit in 38 percent copper alloy showing the arrangement of attachment of side branches to main stem in CuAl. X500 Etch  $\text{HNO}_3$

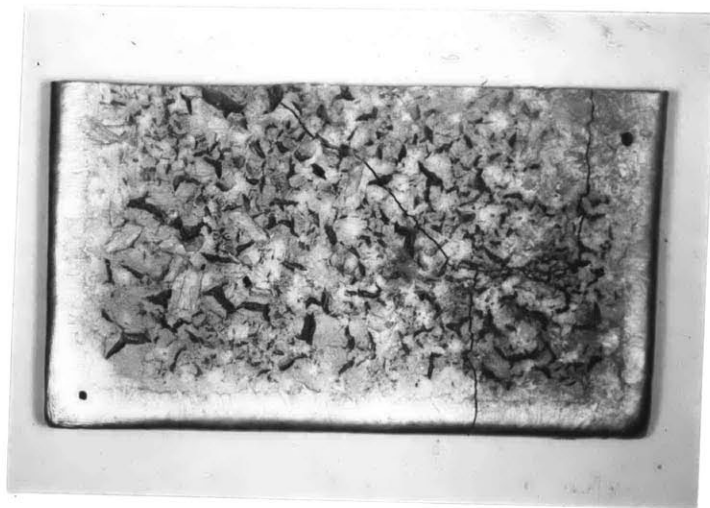


Figure 31: Photograph of 38 percent alloy chill cast plate showing cracks on the top surface which froze last.

Figure 32: Relationship between  $\text{CuAl}_2$  dendrite spacing and freezing rate in 38 percent copper alloy arc deposits.

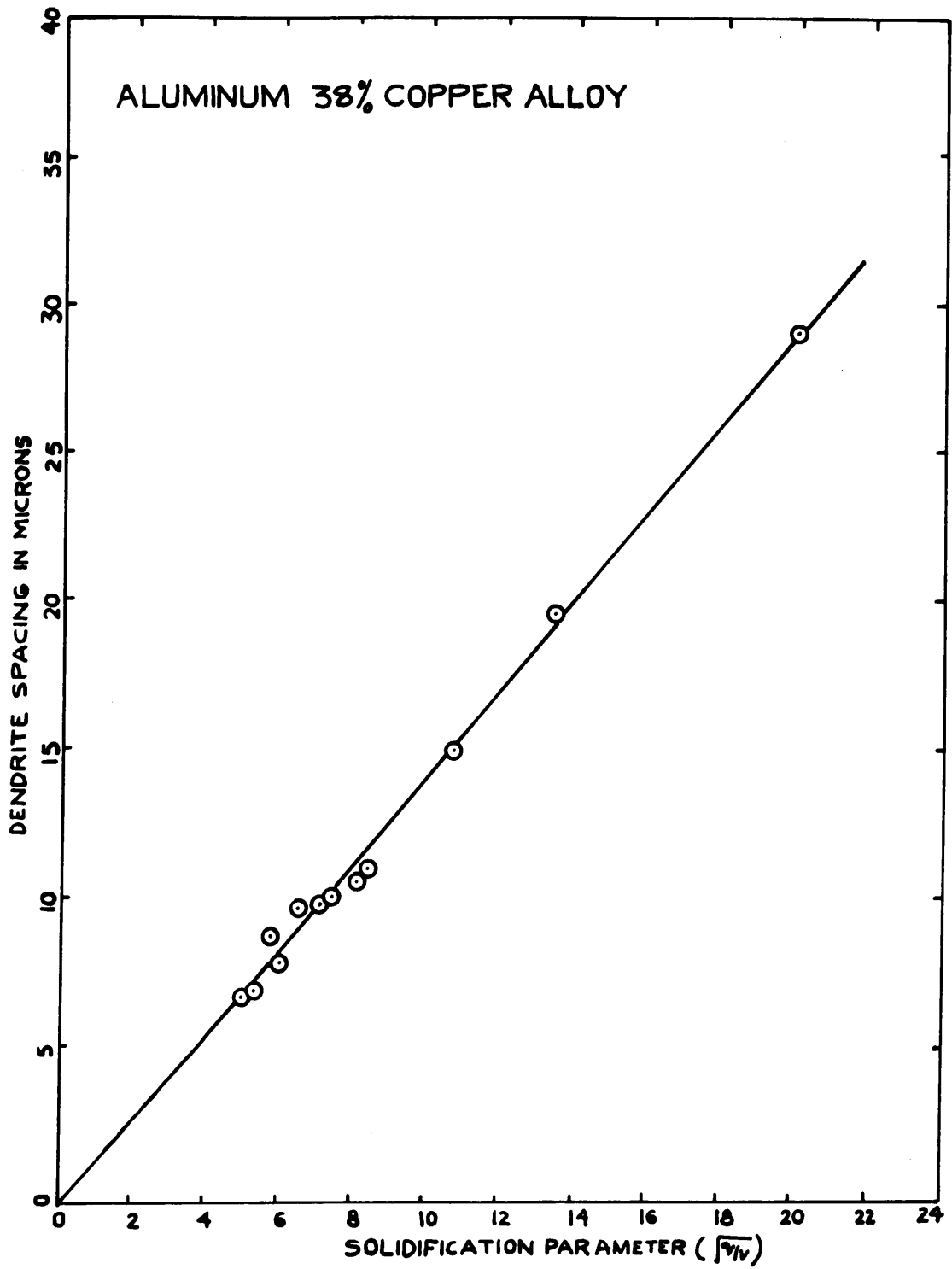




Figure 33: A vertical section through arc deposit in 38 percent copper alloy at  $\sqrt{q/v} = 5$ . X 500 Etch  $\text{HNO}_3$



Figure 34: A vertical section through arc deposit in 38 percent copper alloy at  $\sqrt{q/v} = 20$ . Note the large dendrite spacing compared to Figure 33. X 500 Etch  $\text{HNO}_3$

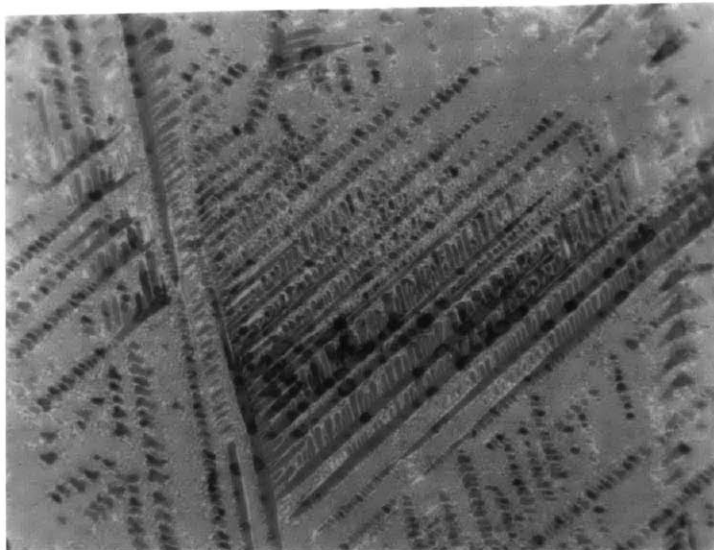


Figure 35: Vertical section of a arc deposit in 38 percent copper alloy showing unusually large secondary arms. Such arrangement was not commonly observed. X500 Etch  $\text{HNO}_3$

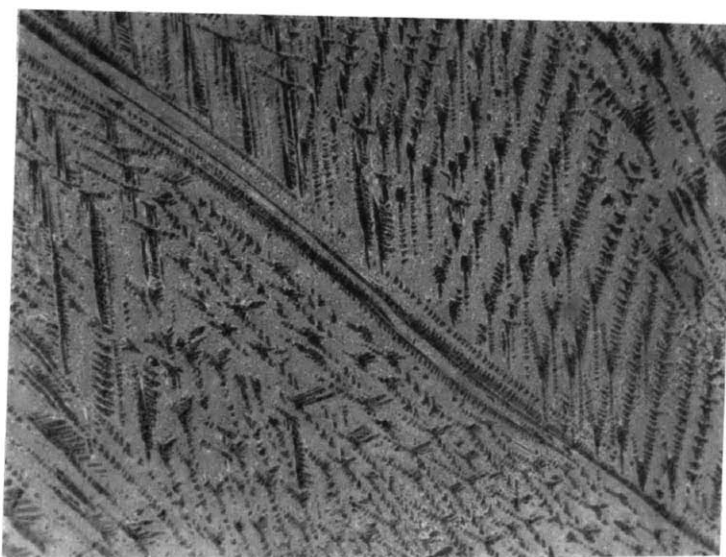


Figure 36: Vertical section of a arc deposit in 38 percent copper alloy showing unusually long dendrites of  $\text{CuAl}_2$  running parallel to each other. X 150 Etch  $\text{HNO}_3$

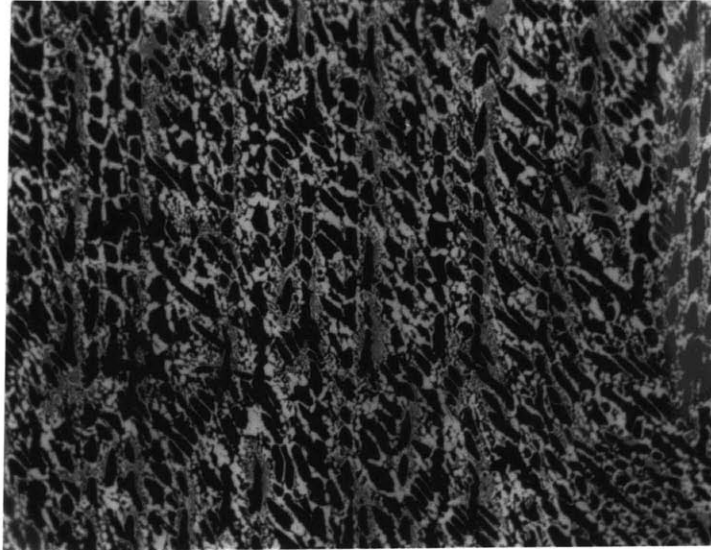


Figure 37: Vertical section through arc deposit of 38 percent copper alloy showing envelope of around  $\text{CuAl}_2$  dendrite. X 50 Etch  $\text{HNO}_3$

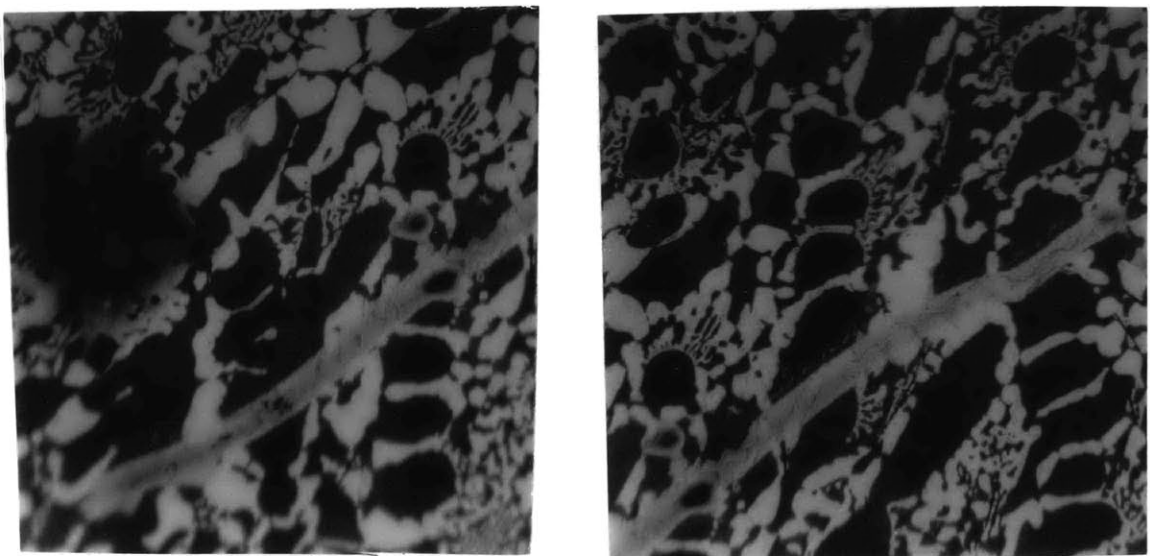


Figure 38: Vertical sections through arc deposit of 38 percent copper alloy showing the trace of electron beam after the electron microprobe analysis. X250 Etch  $\text{HNO}_3$



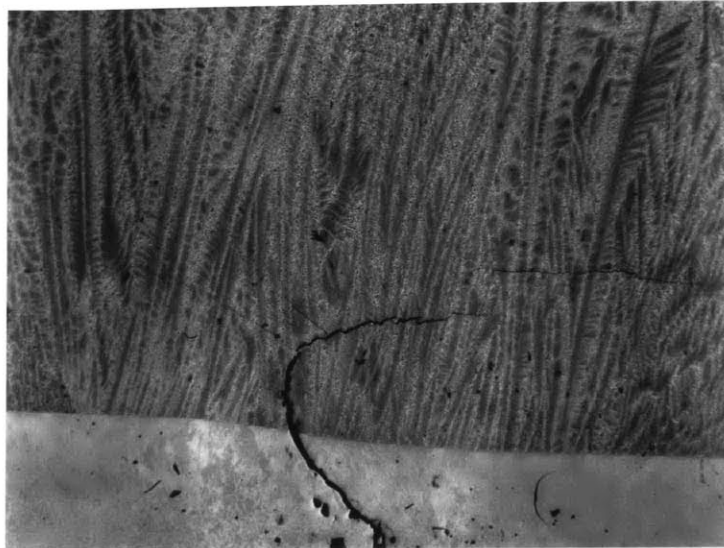


Figure 40: Vertical section through 33 percent copper alloy chilled cast plate showing eutectic arranged in dendritic form. The unresolved position at the bottom shows fine structures of deposit (arc deposit). X13 Etch  $\text{HNO}_3$



Figure 41: Vertical section through slow cooled (plaster cast) ingot of 33 percent copper alloy showing lamellar (unresolvable at this magnification) eutectic arranged in dendritic form with coarse irregular eutectic in between. X13 Etch  $\text{HNO}_3$

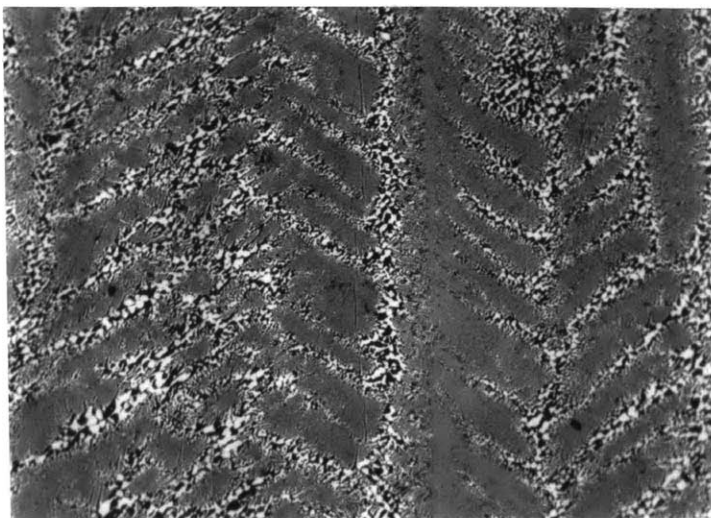


Figure 42: Vertical section through 33 percent copper alloy chilled cast plate showing eutectic arranged in a fir-tree pattern with coarse eutectic in between.  
X50 Etch  $\text{HNO}_3$

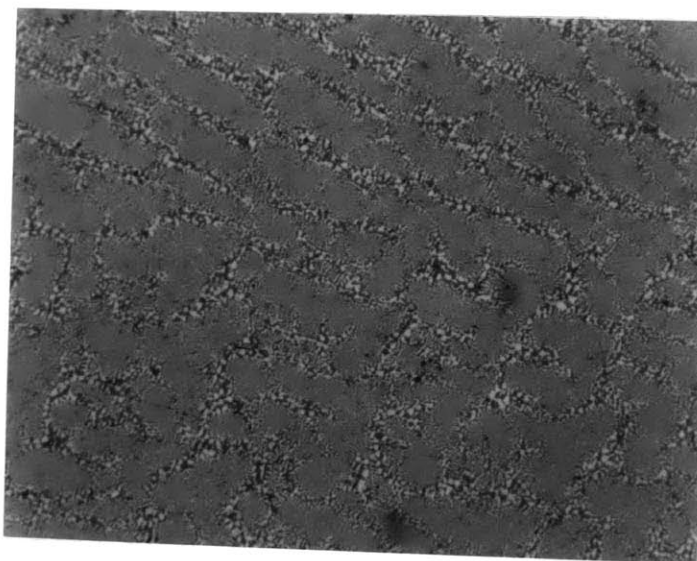


Figure 43: Horizontal section through 33 percent copper alloy chill cast plate showing transverse section of eutectic colonies arranged in dendritic pattern

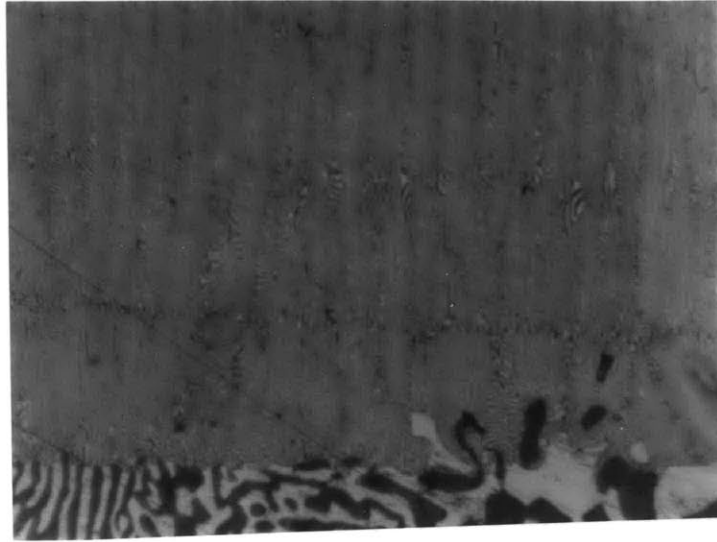


Figure 44: Vertical section through the base of arc deposit in 33 percent copper alloy showing colonies grown perpendicular to the interface. Also note 2 bands running across the picture ( $\sqrt{q/v} = 5$ ). X1000 Etch  $\text{HNO}_3$

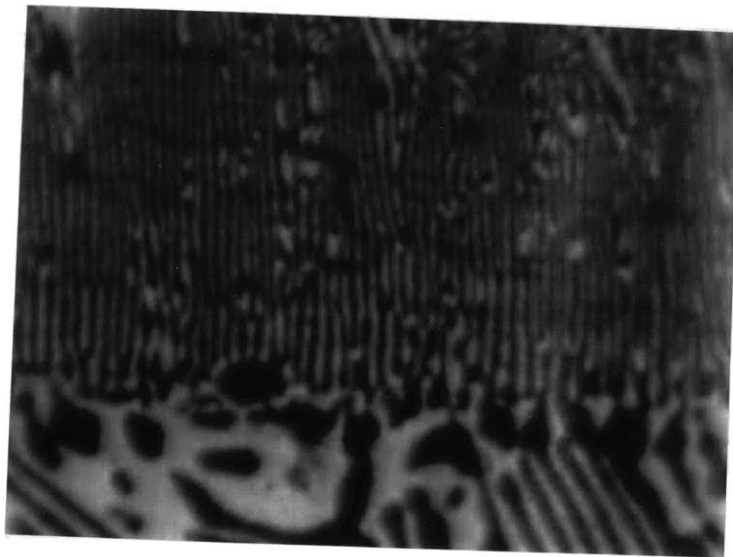
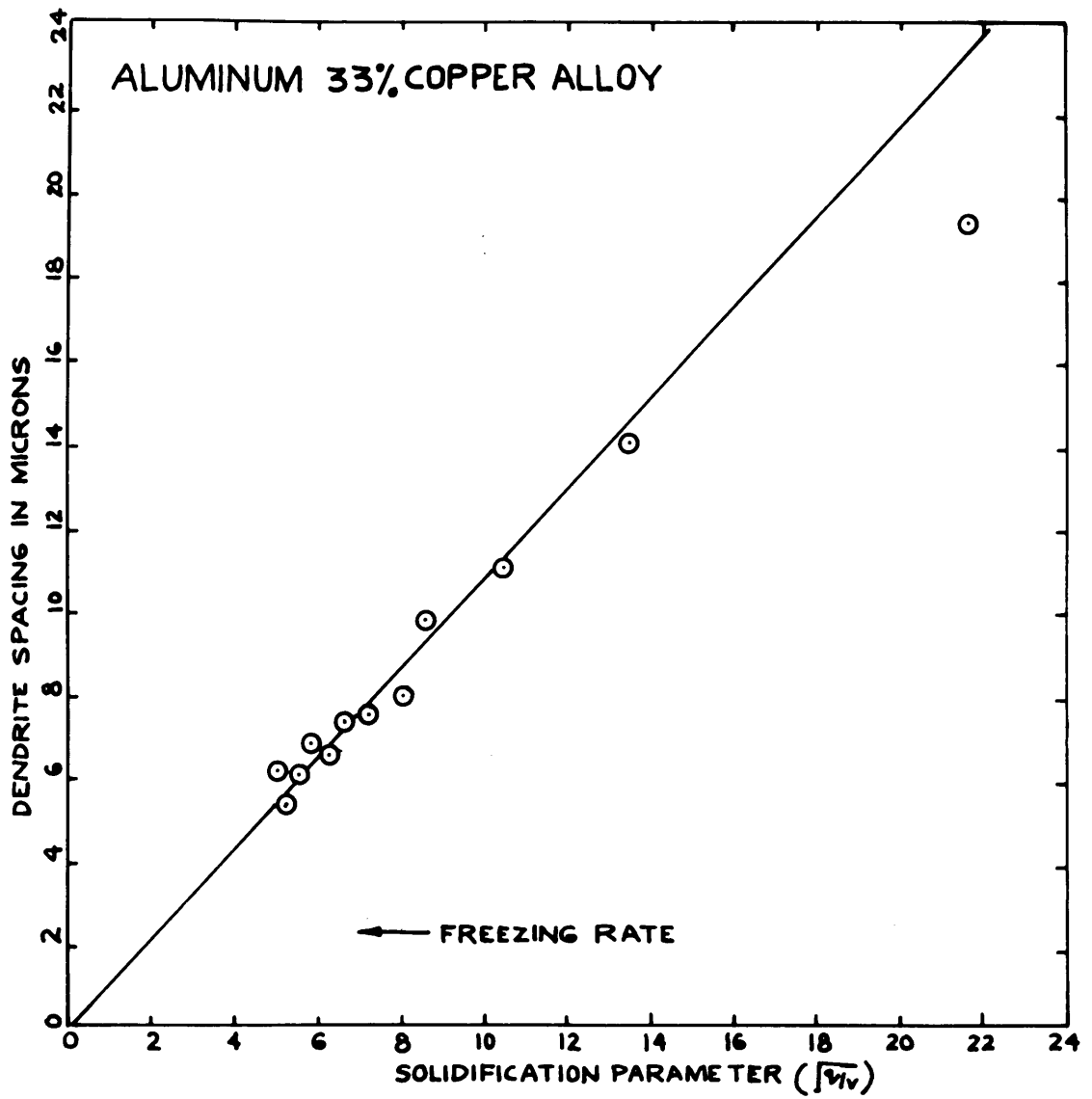


Figure 45: Vertical section near the base of deposit in 33 percent copper alloy showing eutectic lamella grown perpendicular to the interface. X2500 Etch  $\text{HNO}_3$

Figure 46: Variation of colony spacing with freezing rate  
in 33 percent copper (eutectic) alloy arc deposits.



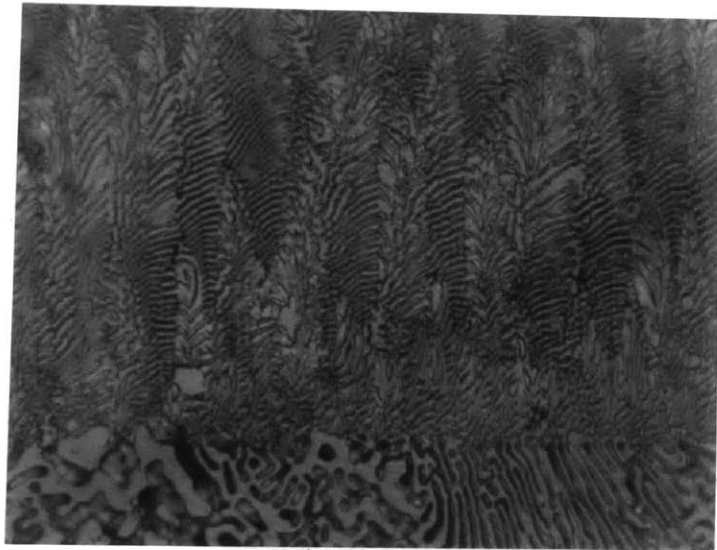
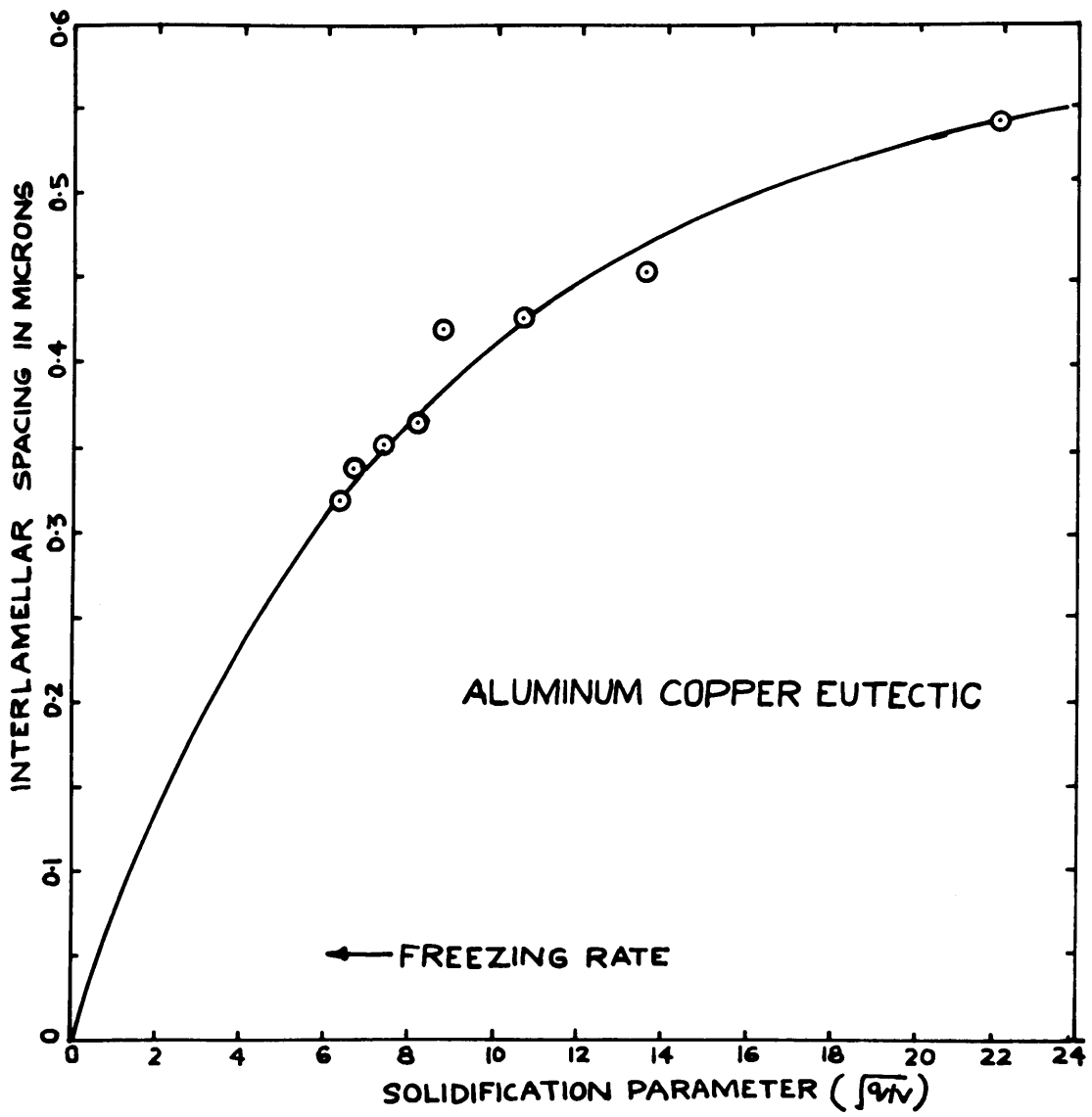


Figure 47: Vertical section through the base of arc deposit of 33 percent copper alloy ( $\sqrt{q/v} = 8$ ) shows colonies grown perpendicular to the interface. Note the coarseness of colonies and lamella compared with those in Figure 44. X1000 Etch  $\text{HNO}_3$

Figure 48(A) Variation of interlamellar spacing with freezing rate in 33 percent copper (eutectic) alloy arc deposits.





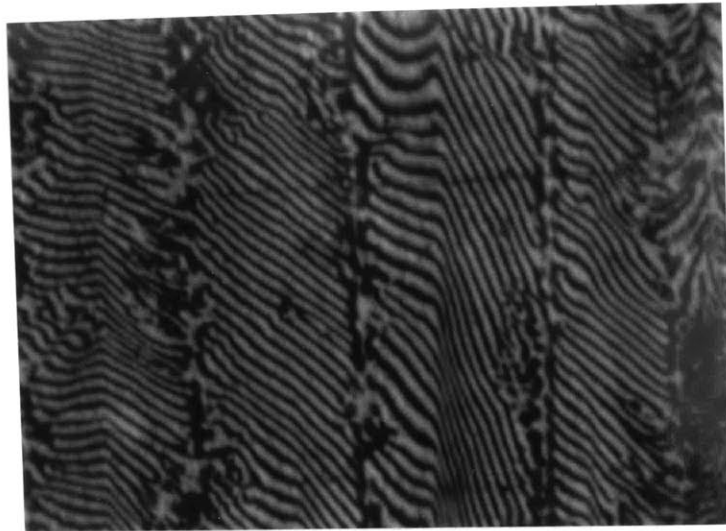


Figure 48: Vertical section through arc deposit in 33 percent copper alloy showing parallel grown colonies. Some of them appear to have bent lamella. X2000  $\text{HNO}_3$

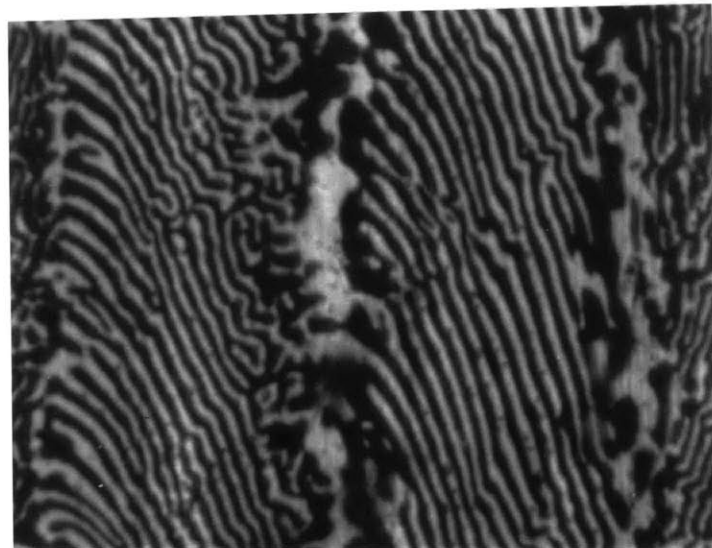


Figure 49: Vertical section through arc deposit in 33 percent copper alloy showing parallel colonies with a layer of phase between them. Also note the defects in lamellar structure, one lamella splitting into two, also discontinuity in certain lamella. X2500 Etch  $\text{HNO}_3$

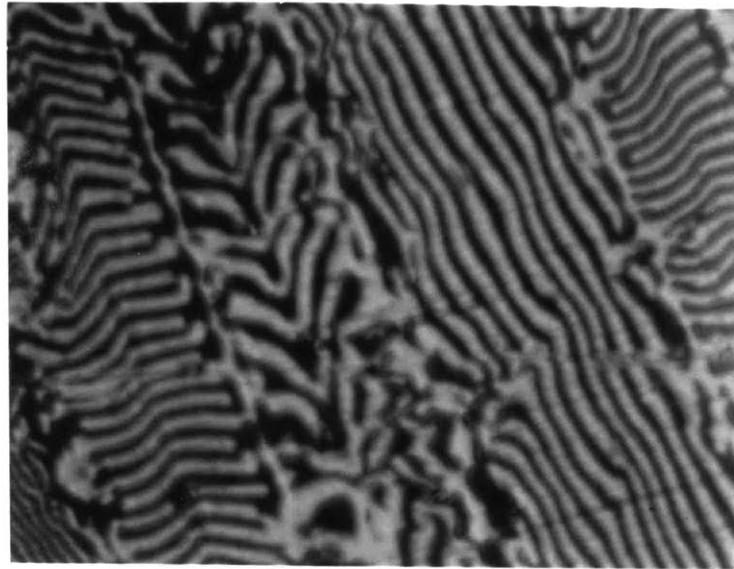


Figure 50: Vertical section through arc deposit in 33 percent copper alloys showing variation in lamellar structure in parallel colonies. One of the colony shows bending of lamella along a certain axis. Two other colonies appear to be grown by a overlapping mechanism<sup>14</sup>. X2500 Etch  $\text{HNO}_3$

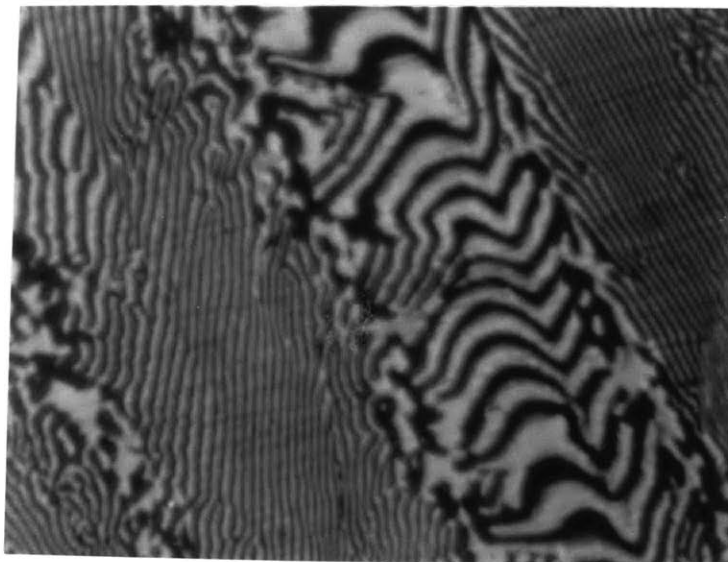


Figure 51: Vertical section through arc deposit in 33 percent alloy shows coarse lamellar arrangement of eutectic in between two colonies. Here also lamella appear to be bent around a certain axis. X2500. Etch  $\text{HNO}_3$

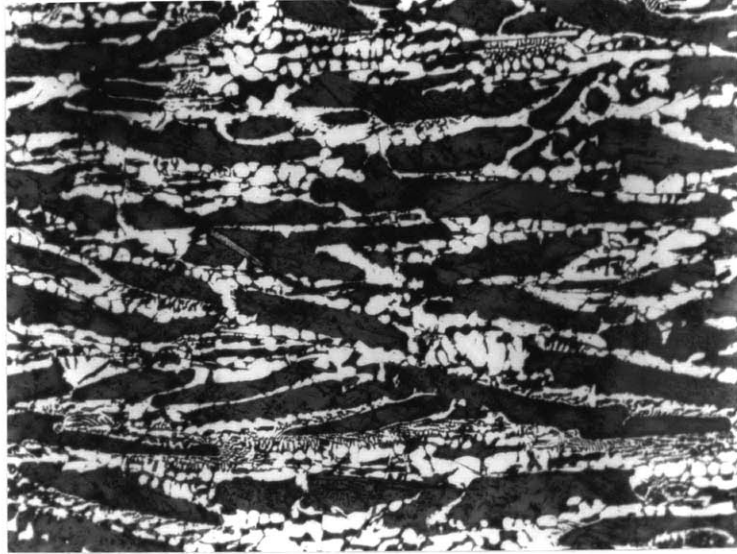


Figure 52: Vertical section through directionally slow cooled 38 percent copper alloy ingot showing coarse dendrites of  $\text{CuAl}_2$  without any side branching surrounded by large  $\alpha$  phase envelopes.  
X50 Etch  $\text{HNO}_3$

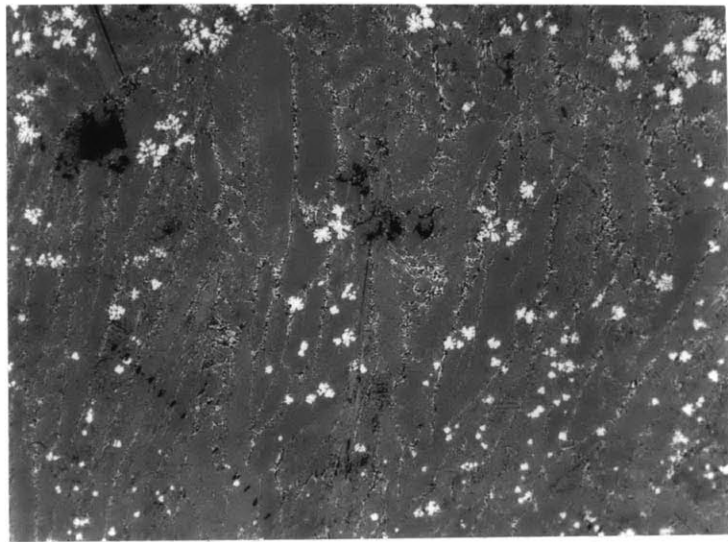


Figure 53: Vertical section along direction of flow (shown by arrow) of solid strip collected during freezing in flowing stream of 33 percent copper alloy showing colonies grown upstream.

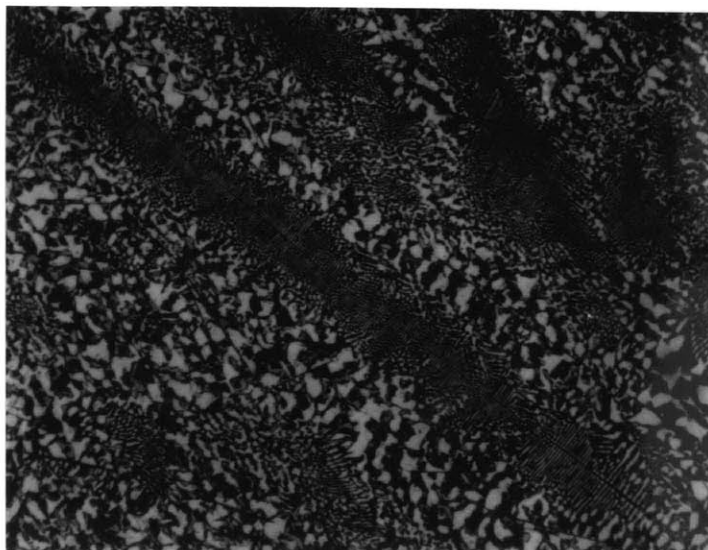


Figure 54: Vertical section through slow cooled (plaster cast) ingot of 33 percent alloy showing eutectic colony with a continuous  $\text{CuAl}_2$  platelet along its length with lamella on both sides. Note coarse eutectic outside the colony. X50 Etch  $\text{HNO}_3$

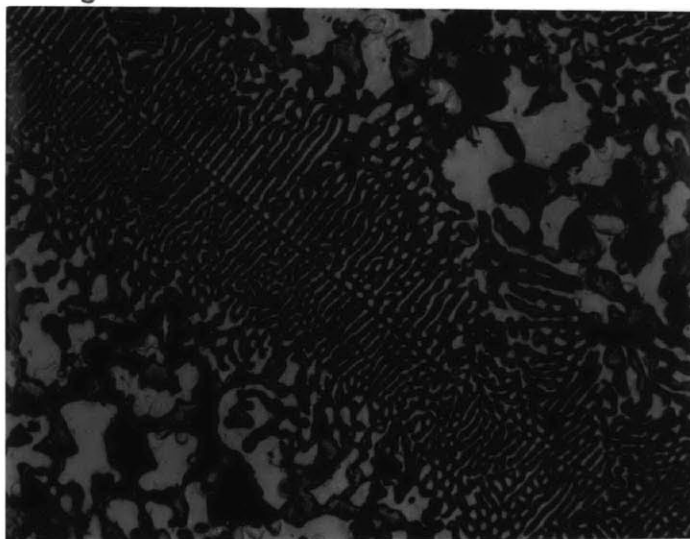


Figure 55: Shows the colony in Figure 52 at a higher magnification. Note the discontinuity in the  $\text{CuAl}_2$  platelet and also thinning of lamella at junctions to this plate. X200 Etch  $\text{HNO}_3$

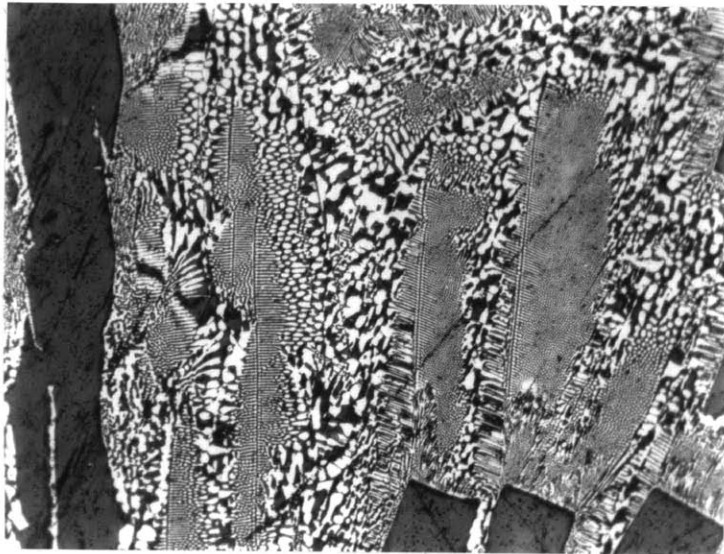


Figure 56: Vertical section through directionally slow cooled ingot (plaster cast) of 38 percent copper alloy showing dendrites of  $\text{CuAl}_2$  with eutectic in between. Note the continuous platelet of  $\text{CuAl}_2$  in the eutectic colonies. X50 Etch  $\text{HNO}_3$



Figure 57: Vertical section through directionally slow cooled ingot of 38 percent copper alloy. Note the tendency of  $\text{CuAl}_2$  to arrange itself in dendritic form with side branches. Behaviour like anomalous eutectic appears to be the cause. X40 Etch  $\text{HNO}_3$

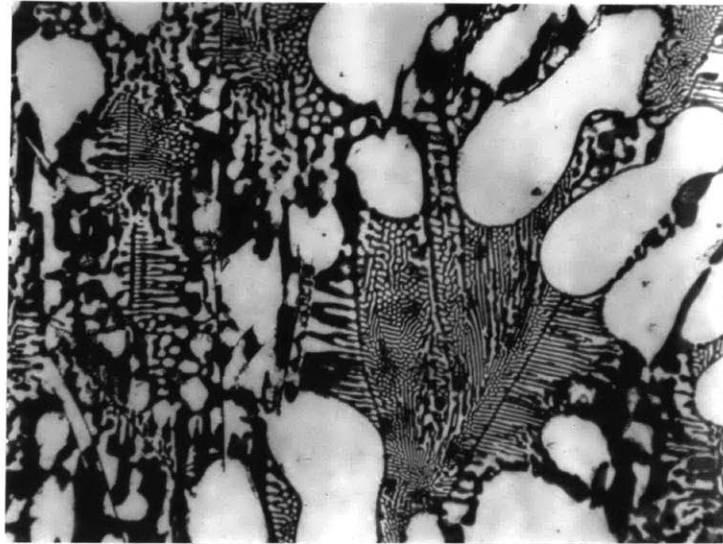


Figure 58: Vertical section through directional slow cooled 24 percent copper alloy ingot (plaster cast) showing primary  $\mathcal{L}$  surrounded by a thin boundary of  $\text{CuAl}_2$  and interdendritic eutectic with long continuous  $\text{CuAl}_2$  platelets.  
X50            Etch  $\text{HNO}_3$

## IX. BIBLIOGRAPHY

1. W. C. Winegard, *Metallurgical Reviews*, 1961, v. 6, 21, 57.
2. D. D. Saratovkin, *Dendritic Crystallization*, Consultant Bureau, Inc., New York, 1959.
3. J. W. Rutter and B. Chalmers, *Canad. Jl. of Physics*, 1953, 31, 15.
4. F. Weinberg and B. Chalmers, *Canadian Jl. Physics*, 1951, 29, 370.
5. D. Walton and B. Chalmers, *Trans. Met. Society, AIME*, 1959, 215, 447.
6. G. Haroy and J. W. Cahn, *Acta Met.*, v. 9, 1961, p. 695.
7. P. E. Brown, Sc. D. Thesis, Dept. of Met., MIT, 1960.
8. D. N. French, Sc. D. Thesis, Dept. of Met., MIT, May, 1962.
9. F. L. Brady, *J. Institute of Metals*, 1922, 28, 369.
10. A. M. Protevin *Ibid*, 1923, 29, 239.
11. L. M. Hogan, *J. of the Australian Institute of Metals*, 1961, v. 6, 4, 279.
12. P. S. Vadilo, *Growth of Crystals*, Moscow Conference, 1956, Consultants Bureau, Inc., p. 109.
13. Ya. V. Grenchy, *Ibid*, p. 65.
14. W. A. Tiller, *Liquid Metals and Solidification*, ASM, Cleveland, 1958, p. 276.
15. H. W. Weart and D. J. Mack, *Trans. Met. Society, AIME*, 1961, v. 221 95.
16. R. W. Craft and D. L. Albright, *Trans. Metallurgical Society, AIME* February 1961, v. 221, 95-102.

17. H. S. Carslaw and J. C. Jaeger, Conduction of Heat Through Solids, Clarendon Press, Oxford, 1959.
18. C. M. Adams, Jr., the Welding Journal, 37, (5), Research Suppl., 210-S (1958).
19. W. G. Pfann, Liquid Metals and Solidification, ASM, Cleveland, 1958, 218.
20. J. Crank, Mathematics of Diffusion Clarendon Press, Oxford.
21. Kellar, Metals Progress, 1944, 46, 806.
22. B. E. Rossi, Welding Engineering, McGraw Hill, New York, 1954.
23. R. Castaing, "Advances in Electronics and Electron Physics", 1960, v. 8, p. 317, Acedemic Press.
24. D. M. Poole and P. M. Thomas, JI. Inst. Metals, Feb. 1962, v. 90, 228.
25. R. F. Palermo, S. B. Thesis, Metallurgy Dept., M.I.T., Jan. 1962.
26. W. Y. Yodelus, J. V. Macewan and J. S. Kirkaldy, "Physical Chemistry of Process Metallurgy", Part II, Interscience Publishers, 1960, 865.
27. R. F. Mehl, The Solidification of Metals and Alloys, AIME, New York, 1951, 46.
28. J. H. Holloman and D. Turnbull Ibid, p. 1.
29. R. W. Craft, Trans. Met. Soc., AIME, Feb. 1962, v. 224, 65.
30. J. P. Chilton and W. C. Winegard, JI. Inst. Metals, Jan. 1961, 162.
31. M. C. Flemings, C. M. Adams, E. E. Huccke, and H. F. Taylor, A.F.S., Trans, 1956, v. 64, 636.



32. D. V. Ragone, C. M. Adams, and H. F. Taylor, *Ibid.*, 653.